Snow dynamics influence tree growth by controlling soil temperature in mountain pine forests

Alba Sanmiguel-Vallelado[1], J. Julio Camarero[1], Enrique Morán-Tejeda[2], Antonio Gazol[1], Michele Colangelo[1,3], Esteban Alonso-González[1], Juan Ignacio López-Moreno[1]

[1] Pyrenean Institute of Ecology, CSIC (Spanish Research Council), Avda. Montañana 1005, 50059 Zaragoza, Spain

[2] Department of Geography, University of the Balearic Islands, Carr. de Valldemossa km 7.5, 07122 Palma de Mallorca, Spain

[3] School of Agricultural, Forest, Food and Environmental Sciences, University of Basilicata, viale dell'Ateneo Lucano 10, 85100 Potenza, Italy

Corresponding author:

Alba Sanmiguel-Vallelado

albasv@ipe.csic.es

Abstract

Snow dynamics are key to understanding tree growth in mountain forests and future response to climate change. However, precise monitoring of microclimate conditions and variables related to tree growth and functioning are lacking. To advance on those issues, snow cover and microclimate conditions, tree phenology, xylogenesis, intra-annual radial growth and the concentration of sapwood and needle non-structural carbohydrates were intensively monitored in four *Pinus uncinata* forests along an altitudinal gradient over three years in a Pyrenean valley (NE Spain). Snow dynamics exerted strong influence on soil temperature and moisture, particularly before and during the early growing season. Soil temperature was the most relevant microclimate variable during the overall xylogenesis, mainly influencing the production of mature tracheids. Large snow accumulation resulted in later snow depletion and a consequent delay in soil warming onset. Low soil temperatures in the spring, related to prolonged snow persistence, retarded cambial reactivation and led to lower growth rate. Despite strong spatial variability among plots, wood production was determined by snow dynamics in three out of the four studied plots. This study highlights the major role played by early and late growing season soil temperatures on radial growth of mountain conifers. The results of this study suggest that a future shallower and more transitory snowpack in the studied forests, together with warmer soil and air temperatures, may increase radial growth and productivity of similar mid-latitude, young mountain forests.

47 **Keywords:** Pyrenees; snow cover; soil temperature; subalpine forests; tree
48 growth; xylogenesis.
49

1. Introduction

Climate plays a major role as driver of forest productivity, stem wood formation and radial growth (Babst et al., 2019). In mountainous areas, regional climate is greatly controlled by topographic complexity (elevation, aspect, slope) and also by the presence of forest patches, resulting in the creation of large microclimatic variability (Albrich et al., 2020; Dan Moore et al., 2005). In cold, high-elevation forests and alpine treelines, low air and soil temperatures limit tree growth by shortening the growing season and reducing growth rates (Körner, 2012). There is a minimal air temperature threshold for cambial activity of many conifers around 5 °C (Rossi et al., 2008). Air temperatures can also impact tree growth by retarding or accelerating snowmelt (Barnett et al., 2005). Snow dynamics have been reported to influence forest productivity, radial growth and xylogenesis in subalpine and subarctic forest ecosystems (Carlson et al., 2017; Helama et al., 2013). A deep snowpack, together with low air temperatures, can delay the melt-out date, resulting in later soil warming, delayed root growth and cambial onset, thus reducing growth (Kirdyanov et al., 2003; Rossi et al., 2011; Vaganov et al., 1999). Other studies, however, have not found that soil temperature strongly influences stem growth and, in such cases, air temperature was considered to be the main factor limiting xylogenesis (D'Orangeville et al., 2013; Lupi et al., 2012; Rossi et al., 2007). Additionally, snowmelt enhances water infiltration into deep soils (Woelber et al., 2018) and can positively influence tree growth by reducing soil moisture-limitation in seasonally dry mountain areas from mid to low latitudes (St. George, 2014; Watson and Luckman, 2016; Zhang et al., 2019).

Mountain forests from mid to high latitudes, where growth is mainly controlled by low temperatures, are very exposed to climate warming (Albrich et al., 2020). Rising air temperatures are expected to promote tree growth by extending the growing season and increasing growth rates (Camarero et al., 2017; Zhang et al., 2017). A likely shallower shorter-lived snowpack in mid-latitude mountain ranges (Beniston, 2012; McCabe and Wolock, 2009; Morán-Tejeda et al., 2017; López-Moreno et al., 2017) will allow the soil temperature to rise earlier in the year, consequently prolonging the growing season. However, a shorter-lived snowpack may also lead to less available snowmelt water at the end of spring, intensifying periods of water shortage in drought-prone regions such as the Mediterranean mountains (Pederson et al., 2011; Truettner et al., 2018).

Understanding how snow dynamics affect tree grow in mountain forests will allow us to anticipate their future responses to forecasted climate change. That is especially relevant in the Spanish Pyrenees, which is a mountain range located in the transition of temperate-continental Atlantic-Eurosiberian and dry Mediterranean climate influences (Del Barrio et al., 1990; El Kenawy et al., 2011; López-Moreno et al., 2010; Morán-Tejeda et al., 2017). This study investigates how seasonal dynamics in snowpack characteristics modify microclimatic conditions (soil temperature and moisture) and tests if these modifications influence intra-annual growth and functioning in Mountain pine (*Pinus uncinata*). For that purpose, microclimate conditions, shoot and needle phenology, xylogenesis, radial growth, sapwood and needle non-structural carbohydrate (NSC) concentrations were monitored in four *P. uncinata* forests situated along altitudinal gradients over three consecutive years in a Pyrenean valley. The objectives of the study were (1) to determine the extent to which small-scale variations in soil temperature and

moisture are influenced by snowpack magnitude and duration; (2) to characterize seasonal growth and functioning in *P. uncinata*; and (3) to analyze the influence of intra-annual snow dynamics on *P. uncinata* growth through snowpack contribution to microclimate. The main hypothesis is that snow dynamics influence intra-annual growth patterns through their impact on soil temperature and moisture.

2. Data and methods

2.1. Study species

The Mountain pine (*Pinus uncinata* Ram.) is a long-lived and shade-intolerant conifer which dominates in high-elevation areas of the Pyrenees, western Alps, and Iberian System (Cantegrel, 1983). Spain's geographical distribution is limited to the subalpine forests of the Pyrenees (1600 - 2500 m) and to two isolated populations in the Iberian System, where it reaches its southern distribution limit (Ruiz de la Torre and Ceballos, 1979). *P. uncinata* begins to form the annual tree ring in April-May and ends growing in October, with main growth peaks from May to July (Camarero et al., 1998). A positive effect of warm air temperatures during the autumn before ring formation and during the growing season has been widely reported in tree-ring studies.(Andreu et al., 2007; Camarero et al., 1998; Galván et al., 2014; Tardif et al., 2003). In addition, there is evidence that a preceding abundant snowpack negatively influences *P. uncinata* radial growth at inter-annual scale (Sanmiguel-Vallelado et al., 2019).

2.2. Study site

The study was performed in the central Spanish Pyrenees (Figure 1a), where climate is continental (Del Barrio et al., 1990). The experimental setting comprised four forest stands located in the Balneario de Panticosa valley (Figure 1b); all stands have different elevations (from 1674 to 2104 m a.s.l.), exposure, forest structure and microclimatology because of the complex topography in this area (see Table 1 and Figure 1c). During the study period, the average annual sum of precipitation registered in the valley bottom (1630 m) was 1493 mm. In each forest an experimental plot of approximately 450 m^2 was designed. The plots were labeled (plot 1, plot 2, plot 3 and plot 4) based on their locations in the valley (from N to S). *P. uncinata* dominates the studied stands, although plot 3 contained a few individual *Pinus sylvestris* L. At each experimental plot, five young individual *P. uncinata* were monitored and their diameter at breast height (Dbh_0) and full height were measured using tapes and clinometers, respectively.

Table 1. Topography, microclimate conditions, tree characteristics, and forest structure in the four plots. Mean ± standard deviations are presented.

Plot	Elevation (m a.s.l.)	Aspect	Slope (º)	DJF air T (°C)	TGS air T (ºC)	Max SD (cm)	MAM GSI ($W \cdot m^{-2}$)	Dbh_0 (cm)	Height (m)	Age (years) †	Density ($indiv \cdot ha^{-1}$)	Basal area ($m^2 \cdot ha^{-1}$)
1	2008	S	29.4	-0.5	11.1	133.2	154	20.4 ± 4.0	9.2 ± 0.3	38 ± 6	1689	45.1
2	1814	E	20.4	-0.4	11.4	169.3	168	18.8 ± 4.6	8.6 ± 1.2	35 ± 7	844	13.7
3	1674	W	9.3	0.3	12.2	95.3	193	22.4 ± 2.9	9.5 ± 1.1	42 ± 4	533	35.3
4	2104	NE	22.7	-2.0	10.3	260.4	195	20.2 ± 4.0	9.1 ± 0.3	37 ± 6	356	26.6

Abbreviations: DJF T, winter mean air temperature from December to February; TGS, Thermal Growing Season (see 2.4 section); Max SD, maximum snow depth; MAM GSI, average global solar irradiation from March to May; Dbh_0, diameter at breast height at the beginning of the study. Note: The methods used to obtain stand structure data were described in Sanmiguel‐Vallelado et al., (2020). (†) Tree age was estimated from Dbh_0 values based on an age-Dbh linear regression constructed in a nearby *P. uncinata* forest.

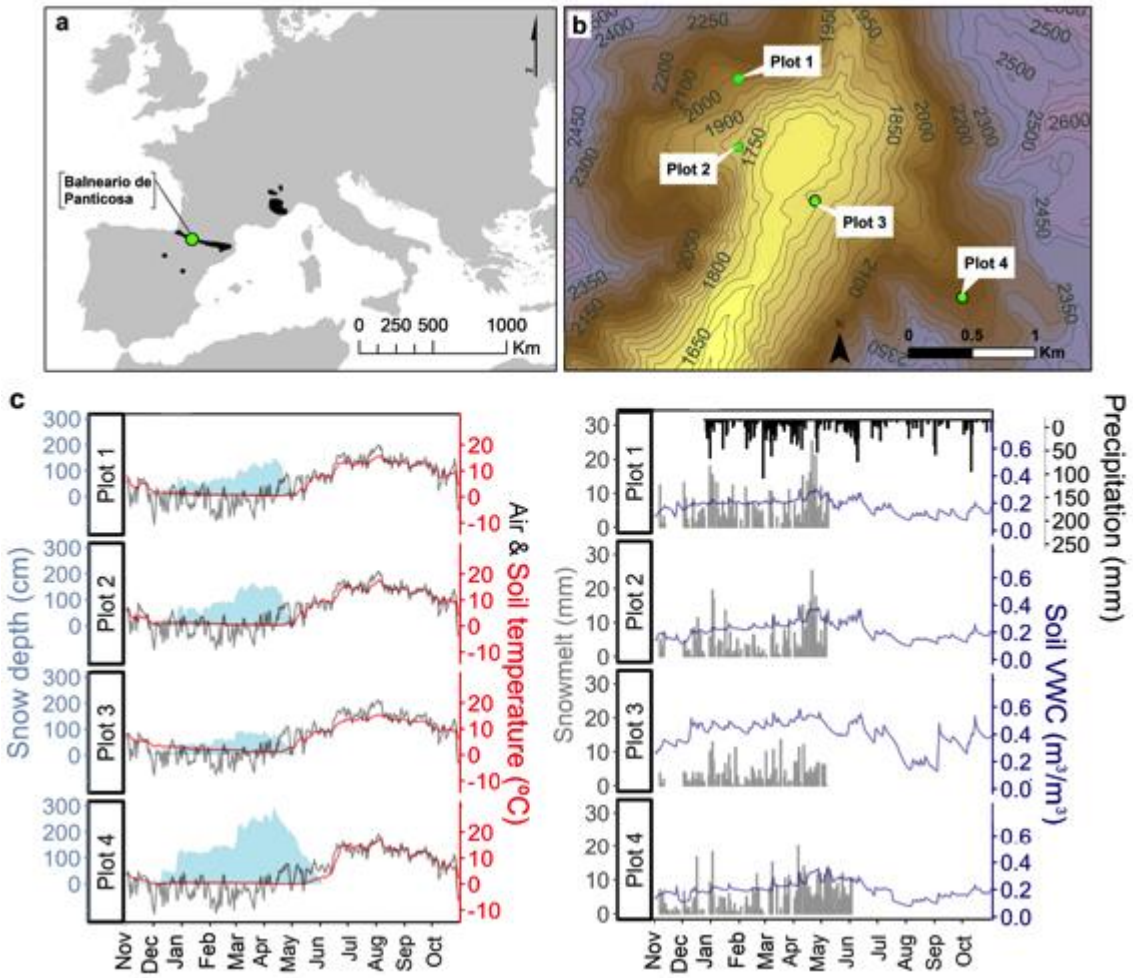

Figure 1. (a) Distribution of the study species (*Pinus uncinata*) in Europe (black areas) and location of the study area location (Balneario de Panticosa) in the Spanish Pyrenees (green dot). (b) Location of the experimental plots in the study valley. (c) On the left: daily time series of snow depth (light blue areas), mean soil temperature (red lines) and mean air temperature (grey lines) by plot during 2018. On the right: daily time series of snow melting rates (grey bars), mean soil VWC (blue lines), and precipitation sum (black bars) by plot during 2018. Precipitation data source was a meteorological station located in the study area at 1630 m a.s.l. (note that this series contained NA periods).

2.3. Data collection

A graphical description of the monitoring procedures and measures variables is shown in Figure A.1.

2.3.1. Microclimate data

Air temperature (T) and humidity (H) series were obtained using dataloggers (Tinytag-Plus-2; model TGP-4017, Gemini DataLoggers UK Ltd., Chichester, West

Sussex, UK) that were equipped with naturally ventilated radiation shields (Datamate ACS-5050 Weather Shield; Gemini DataLoggers UK Ltd., Chichester, West Sussex, UK). One datalogger was installed at each plot stand, hanging from a tree branch, and measurements were recorded every 15 minutes from November 2015 to December 2018.

The soil temperature (T soil) series was obtained using miniature temperature loggers (Thermochron iButton; DS-1922L model, Dallas Semiconductors, Texas, USA). Four to six dataloggers were installed at each studied forest stand in a distributed manner, covering both forest openings and beneath forest canopy areas. The dataloggers were wrapped with laboratory film and duct tape to prevent corrosion, tied to metallic picks to facilitate their later retrieval, and buried in the ground at a depth of 10 – 20 cm. Soil temperature data were collected every hour from November 2015 to December 2018.

The soil moisture series was obtained using ECH_2O probes (EC-5 model, Decagon Devices, Pullman, WA, USA). Soil moisture sensors were installed in a distributed manner at each plot: two sensors were installed in forest openings and two beneath forest canopy areas. Sensors were buried in the ground at a depth of 10 - 20 cm. Volumetric water content (VWC) of soil was registered by the ECH_2O datalogger every 1.5 hours from November 2015 to December 2018. The first month of measurements was discarded in order to ensure a proper settling time after field installation.

Snowpack data were collected from November 2015 to June 2018. Each year comprised snow data collected from the onset of snow accumulation to the end of melting. The snow depth series was obtained from automatic time-lapse cameras

(Bushnell, Trophy Cam, Kansas, USA) shooting every day at eight fixed snow poles at each plot: three poles were placed in an open area and five were placed beneath the forest canopy at each plot. Photographs were processed using ImageJ software (Rasband, 1997) to manually obtain a daily snow depth series. The average daily snow depth series for the set of poles at each experimental plot was calculated. Snow Water Equivalent (SWE) was manually surveyed every 10 to 15 days using a snow cylinder and scale (ETH core sampler, Swiss Federal Institute of Technology, Zurich) at snow pits dug at two single locations in each plot, one in a forest opening and one below the forest canopy. Two replicates per location were collected. Snow density data was calculated from SWE collected data using the equation (Eq. 1):

$$\rho_s = \frac{SWE \cdot \rho_w}{H} \qquad (1)$$

where ρ_s is the snowpack density ($kg \cdot m^{-3}$), SWE is the measured equivalent water of the snowpack (m), H is the measured snowpack depth (m), and ρ_w is the assumed water density ($kg \cdot m^{-3}$). Daily snow density series were estimated by linear interpolation between each pair of density measurements from consecutive surveys. Daily SWE series for the set of poles at each experimental plot were inferred from data on daily snow depth and estimated daily snow density. The methodology to obtain the snow dataset is described in Sanmiguel-Vallelado et al. (2020).

2.3.2. Stem radius variations

Changes in stem perimeter were monitored on two to three individual *P. uncinata* at each plot, using stainless-steel band dendrometers (DR 26, EMS Brno, Czech

209 Republic). Dendrometers (n = 10) were installed at a height of ~ 150 cm on the
210 individual stems. The external layer of dead bark was previously removed. Hourly
211 stem perimeter variations data (1 µm resolution) were collected from April 2016
212 to December 2018 and transformed into radial changes, assuming a circular shape
213 of the stem and measuring the diameter at breast height (1.3 m) at the beginning
214 of the study (Dbh_0). Data downloading (Mini 32 software, EMS Brno, Czech
215 Republic) was done seasonally (i.e. four times per year, every three months).

216

217 *2.3.3. Xylogenesis*

218 To study xylogenesis (xylem phenology and development), wood samples
219 (microcores of 2 mm diameter and 15-20 mm length) were collected from five
220 individual *P. uncinata* at each plot to monitor wood formation. Microcores (n = 20)
221 were taken weekly or bi-weekly from May to October during 2016 and 2017. The
222 individuals were punched with a Trephor® increment puncher at 1-1.5 m height,
223 following an ascending spiral pattern, and each sample was taken at least 5 cm
224 from previous sampling points (Deslauriers et al., 2015). The samples usually
225 contained the preceding 4–5 rings and the developing ring with the cambial zone
226 and adjacent phloem. Microcores were immediately fixed in 50% ethanol solution
227 and preserved.

228 Transversal wood sections (15-20 µm thick) were obtained using a sliding
229 microtome (Leica SM2010 R) with temperature Controlled Freezing Stages for
230 Microtomes (Physitemp BFS-30MP), which allowed freezing the samples for
231 optimal sectioning. Sections were mounted on glass slides, stained with 0.05%
232 cresyl violet and fixed with Eukitt®. The mounted and fixed sections were
233 examined with visible and polarized light within 10–30 min of staining. Images of

sections were first taken at 40–100x magnification, using a digital camera mounted on a light microscope (Olympus BH2, Olympus, Hamburg, Germany). We counted and averaged, on five radial lines per ring, the number of cambium cells, radially enlarging tracheids, wall-thickening tracheids and mature cells (Camarero et al., 2010; Deslauriers et al., 2015). Images allowed verifying cell counts and distinguishing earlywood (EW) and latewood (LW) tracheids according to their lumen and cell wall thickness, distinguishing earlywood from latewood tracheids as a function of their radial lumen diameter and wall thickness following (Denne, 1989). In the developmental stage, cells showed different shapes and stained with different colors (Antonova and Stasova, 1993); cambial cells had similar and small radial diameters and thin walls; radially elongating tracheids showed a wider radial diameter and contained a protoplast enclosed by a thin primary wall; wall-thickening tracheids corresponded to the onset of secondary cell wall formation and were characterized by cell corner rounding; secondary walls glistened under polarized light and walls turned blue due to wall lignification; and mature cells did not contain cytoplasm and presented completely blue walls.

2.3.4. Shoot and needle phenology

Following the procedure reported in Rossi et al. (2009) the dynamics of shoot and needle growth on five individual *P. uncinata* were monitored at each experimental plot. Shoot and needle measurements were taken weekly or bi-weekly from May to October during 2016 and 2017. Five lower branches, from all exposures, were selected on each tree. On the branches, the developing apical shoots were measured with a ruler (1 mm precision). On each shoot, five developing needles were randomly selected and measured.

2.3.5. Non-structural carbohydrate concentrations

Non-structural carbohydrate (NSC) concentrations were quantified in stem sapwood and young needles of stems from individual five *P. uncinata* at each experimental plot. Three apical shoots and one core, taken at breast height (1.3 m) with Pressler increment borers (Gestern, Germany), were seasonally collected from selected trees in 2016. The concentrations of soluble sugars (SS) and starch (as non-soluble sugars NS) were measured in current-year needles and stem sapwood. Following Sangüesa-Barreda et al. (2012), SS were extracted with 80% ethanol solution and a colorimetric approach to determine their concentration. The undissolved fraction of carbohydrates after ethanol extraction was enzymatically reduced to glucose and then analyzed, as in Palacio et al. (2007). NSC measured after ethanol extraction is referred to as SS; carbohydrates measured after enzymatic digestion in glucose equivalents are referred to as starch; and the sum of SS and starch is referred to as total NSC (TNC).

2.4. Data analyses

From the raw microclimate series, a few (<1%) outliers caused by errors in sensor measuring were removed. Missing data were estimated using a non-parametric iterative imputation method called missForest (Stekhoven and Buhlmann, 2012), which is implemented in the MissForest R package (Stekhoven, 2013). For each variable, the missForest method fits a Random Forest regression to the observed part and then predicts the missing parts of the input data (Breiman, 2001). Average daily series at each experimental plot were calculated. Data from forest openings and beneath forest canopy areas were averaged for SWE, soil

284 temperature and soil moisture series. Snowmelt was calculated by first-order
285 differencing from SWE daily series. Only snow data in a continuous snowpack
286 period were considered; that is, from the date of the first day of 14 or more
287 consecutive days with snow on the ground (i.e. snow accumulation onset) to the
288 last date with a snow record (i.e. melt-out date). Air warming onset was defined as
289 the day when the 7-day running mean air T reached a threshold of 5ºC after the
290 date of minimum air T, because 5ºC is the minimal temperature threshold for
291 cambial activity of many conifers (Rossi et al., 2008). Soil warming onset was
292 determined the same way, with the soil temperature series. Therefore, the most
293 favorable thermal growing season (TGS) comprises the period when air
294 temperatures overcome the 5ºC threshold. Snowmelt infiltration in soil was
295 assumed when there was a rise of 0.01 $m^3 \cdot m^{-3} \cdot day^{-1}$ of soil VWC (Harpold et al.,
296 2015).

297 Regressions at plot level (i) were performed between monthly sums of
298 snowmelt and monthly averages of soil VWC and (ii) between monthly averages of
299 SWE and soil T to investigate influences of snowpack on soil conditions. Linear and
300 polynomial adjustments were done, respectively. The linear soil VWC response to
301 snowmelt allowed inference of temporal variability of this relationship by
302 performing correlation analysis between snowmelt weekly sums and soil VWC
303 weekly averages, grouping by month and plot. The influence of snow duration on
304 soil T over time was determined by performing correlation analysis between the
305 melt-out date and the (current and following) monthly average values of soil
306 temperature by plot and year.

From xylem development data, the increase in the number of mature tracheids was modelled at plot level with a Gompertz function (Eq. 2) (Zeide, 1993) using the non-linear regression procedure included in the growthmodels R package (Rodriguez Perez, 2013), following Camarero et al. (1998) and Rossi et al. (2003).

$$Y = A * \exp[-\exp(\beta - k * t)] \qquad (2)$$

where Y is the weekly cumulative sum of mature cells (sum of earlywood and latewood mature tracheids), A is the upper growth asymptote, β is the x-axis placement parameter, k is the rate of change parameter, and t is the time in day-of-year (DOY). Adjusted functions were again limited to the main *P. uncinata* growing season period (Camarero et al., 1998). Daily rates of mature tracheids production (Number of mature tracheids ·day^{-1}) were estimated by first-order differencing the values of two consecutive days of the Gompertz-adjusted series.

For the stem radius variations data series, calculating daily mean and maximum values allows removal of the effect of temperature and soil moisture fluctuations on stem diameter changes over daily periods (Deslauriers et al., 2007). However, a daily approach was preferred because the temporal resolution of most available microclimate variables was not high enough to perform further analysis for selecting a stem cycle approach. Dendrometer raw data were processed using the dendrometeR package (van der Maaten et al., 2016) to obtain the daily maximum radius series. Dendrometer data was delimited to the main *P. uncinata* growing period (Camarero et al., 1998), and was set to 0 on April 1 every season (in 2016 the series was set to 0 the May 1 due to data availability). Gompertz functions were adjusted to daily maximum radius series at plot level following the

331 procedure described above (Eq. 2). Daily rates of radial increment (μm·day^{-1}) were
332 estimated by first-order differencing the values of two consecutive days of the
333 Gompertz-adjusted series. Some annual indices were extracted from mature
334 tracheid production, stem radial increment and phenology data to characterize
335 tree growth (see Table A.1.).

336 Intra-annual microclimate effects on tree growth were examined by
337 performing correlation analyses between weekly averages of microclimate
338 variables and weekly maximum growth rates. Correlations were grouped by
339 month and plot. Additionally, principal component analyses (PCA) were performed
340 to identify the most representative microclimate variables of tree growth rates
341 during the whole growing period. The first PCA was performed using weekly
342 microclimate averages and maximum rates of mature tracheid production; the
343 second PCA was performed using weekly microclimate averages and maximum
344 rates of radial increment. A set of non-correlated variables (principal components,
345 PCs) was obtained; these were linear combinations of the original variables
346 (Jolliffe, 2002). The number of PCs selected in each PCA was based on the Kaiser
347 criterion (Kaiser, 1974), preserving those with eigenvalues > 1. The original
348 variables were classified into the selected PCs by following the maximum loading
349 rule. Original variables were represented as vectors, indicating (i) the direction in
350 which the value of the vector increases, and (ii) the correlation magnitude among
351 vectors and between vectors and component axes (low angles correspond to high
352 correlations).

353 The non-parametric Kruskal-Wallis test was used to assess whether there
354 were statistically significant differences in certain variables among plots or years,

(i.e. air and soil temperatures, soil VWC, and NSC concentrations). This test was selected because the assumption of normality in data distribution within the groups of analyzed variables was not always met (Shapiro-Wilk test: $p < 0.05$). If the Kruskal–Wallis test was significant, the Dunn test post-hoc analysis was performed to determine which groups differed from each other. In correlations, Pearson coefficients were calculated when data distribution of the analyzed variables was normal (Shapiro-Wilk test: $p > 0.05$), otherwise, Spearman coefficients were calculated. All analyses were performed using R statistical software (R Core Team, 2018).

3. Results

3.1. Influence of snowpack on microclimate

Snow accumulation occurred from November to January, whereas the snow melt-out dates occurred throughout April and May (DOY 122 ± 21; average value ± SDs among all years and plots), with a snow cover lasting 143 ± 39 days (Table A.2.). Snow accumulation usually peaked in mid-March (DOY 74 ± 25), reaching maximum depths of 120 ± 67 cm. Larger snow accumulation involved later melt-out dates ($r = 0.91$, $p < 0.05$) (Figure A.2.a) and a longer duration of annual snow cover ($r = 0.87$, $p < 0.05$). More variability in snowpack duration and magnitude was found among plots (CV = 0.24, CV = 0.50) than among years (CV = 0.16, CV = 0.29).

Soil temperatures were highly influenced by snowpack magnitude during the snow-covered period. Both variables presented a non-linear relationship (Figure A.3.a); thus, snow presence induced soil cooling until insulation. Snowpacks with more than a 65 cm depth (on average) insulated the ground from

winter air temperatures and, consequently, freezing of the soil surface was very rare. On average, soil temperature was 3.3ºC higher than air temperature during winter. During spring, the snowpack also insulated the ground; in this case, soil temperature was on average 2.8ºC lower than air temperature. Soil warming onset occurred in early May (DOY 125 ± 22), 4 ± 8 days after the melt-out date, and 26 ± 23 days after air warming onset (early April; DOY 99 ± 24) (Table A.2.). Soil warming onset differed among plots (SD = 18 days), contrary to air warming onset (SD = 6 days). Soil warming onset was driven by the melt-out date (r = 0.94, p < 0.05; Figure A.2.b). May and June soil temperature was negatively influenced by melt-out date (Figure A.3.b). There were lagged effects (1 – 2 months) of snow persistence on soil temperature (in May r = -0.76, p < 0.05; in June r = -0.71, p < 0.05). Soil temperature also was correlated to air temperature during these months (in May: r = 0.69, p < 0.05; in June: r = 0.66, p < 0.05). From July onwards, soil temperature was mostly correlated to air temperature.

Soil water infiltration occurred during all snow-covered periods. Soil VWC peaked in late April (DOY 120 ± 17), 46 ± 36 days after the SWE peak, either before (2 ± 28 days) or after (23 ± 27 days) the melt-out date (Table A.2.). No significant correlation was found in timing or magnitude between the soil VWC and SWE peaks. Positive relationships were found between snowmelt and soil VWC on a monthly scale (Figure A.4.a), being more frequent in Plot 1. This influence was stronger when larger melt occurred, i.e. in April and May (Figure A.4.b). No statistically significant correlations were found when lagged effects (1 or 2 months) of snowmelt on soil moisture were analyzed (data not shown).

Different microclimatic conditions were observed across plots and years (Table 1; Table A.2.). Plot 4 showed the longest and thickest snowpacks, and the coldest air and soil temperatures during winter and TGS. Plot 3 showed the shortest and shallowest snowpacks, the warmest winter air temperature and TGS, and the highest soil VWC all year round. Plots 1 and 2 presented similar winter temperature and March snow depth. Plot 2 showed the warmest soil temperature during TGS. Plot 1 showed the lowest soil VWC values during TGS and reached the minimum soil VWC values earlier. In 2018, the longest and deepest snowpack, and the largest soil VWC and air humidity values during TGS were reached. In 2016, significantly warmer air and soil TGS temperatures were observed, whilst during 2017 the opposite was found. In 2017, the shortest snow season and, as a result, the earliest melt-out dates were observed.

3.2. P. uncinata radial-growth characterization

Stem radial increment lasted on average 91 ± 44 days; it began in mid-May (DOY 130 ± 15) and finished in August (DOY 221 ± 33) (Figure 2a; Table 4). Overall, the annual stem radial increment was 1.0 ± 0.7 mm. More variability in the duration of the radial increment period was found among plots (CV = 0.40) than among years (CV = 0.23). More variability in seasonal radial change was also found among plots (CV = 0.75) than among years (CV = 0.21). Based on estimated daily rates of stem radial increment (Figure 2b, Table 4), growth peaked in mid-June (DOY 162 ± 9). Again, more variability was found in the magnitude of maximum rates of radial increment among plots (CV = 0.49) than among years (CV = 0.22).

In 2018, the duration of the radial increment period was longer, the radial increment was higher and rates of radial increment were the lowest, followed by

2017. The maximum rates occurred earlier in 2017 than in other years. Plot 4 showed the longest radial increment periods, the highest and latest rates of radial increment and the largest total radial increment; followed primarily by plot 3. Plot 1 showed the lowest values for the mentioned variables.

The onset of tracheid formation, i.e. when the first enlarging tracheids were formed, occurred in mid-May (Figure 3a). The number of radially enlarging tracheids peaked from mid-May to late June. Tracheid maturation ended in October, when the thickening phase finished. Based on Gompertz models adjusted to the cumulative sum of mature cells, the estimated timing of growth season differed slightly from the previously noted (Figure 3b). The formation of mature tracheids started in early June (DOY 160 ± 7) and finished in October (DOY 286 ± 20) (Table 4). Maximum rates of production of mature tracheids (0.57 ± 0.28 cells day^{-1}) occurred in mid-July (DOY 202 ± 20) (Figure 3c). A high variability was found in the magnitude of maximum rates of production of mature tracheids among plots (CV = 0.51), but not among years (CV = 0.17).

The production of mature tracheids started and peaked earlier in 2017 but lasted longer in 2016 (Figure 3c). Plot 4 showed the longest period of production of mature tracheids, and the highest production rate, followed by plot 3, whereas plot 1 showed the lowest values for the mentioned variables.

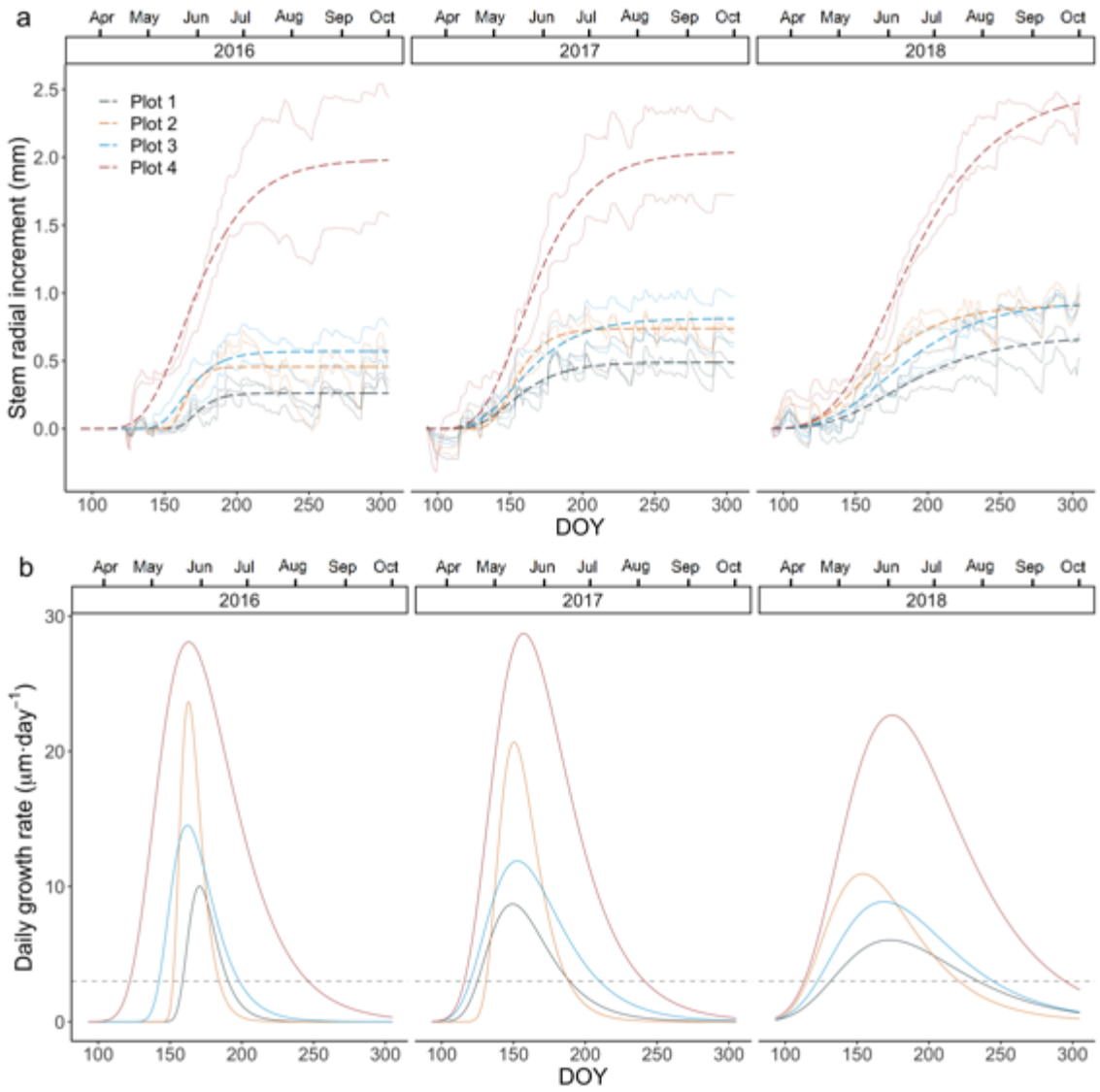

Figure 2. (a) Time series of stem daily maximum radius by tree (solid lines) and same series adjusted to Gompertz function at plot level (dashed lines) during 2016, 2017 and 2018. (b) Estimated daily rates of stem radial increment by plot during 2016, 2017 and 2018. Timing is represented by the day of the year (DOY). Dashed lines in the bottom panels represent daily growth rates equal to 3 µm·day^{-1}.

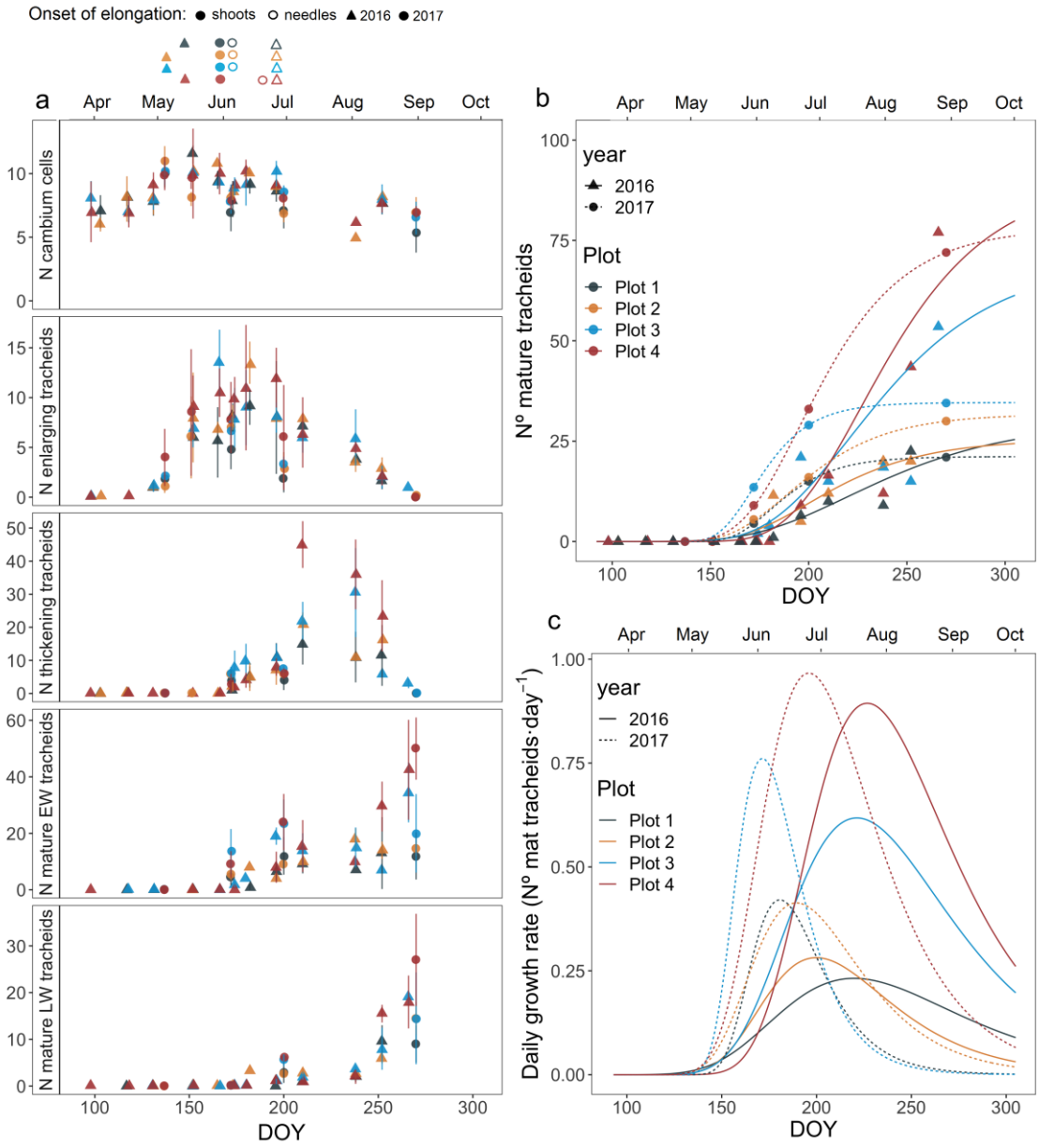

Figure 3. (a) Number of cambial cells and number of tracheids in the radial enlarging, wall-thickening and mature phases during 2016 and 2017. Median values by plot are shown. Bars represent inter-tree variability (standard deviation). Over the top of the plot the onset of shoot and needle elongation for each study plot and year are indicated. (b) Observed (dots) and Gompertz-modelled (lines) function of the number of mature tracheids during 2016 and 2017. (c) Estimated daily rates of production of mature tracheids by plot (daily number of produced mature tracheids) during 2016 and 2017. Timing is represented by the day of the natural year (DOY).

3.3. Needle and shoot phenology

In 2016, the onset of shoot elongation occurred earlier (May) than in 2017 (early June). A 55% smaller shoot length was reached in 2016 than in 2017 (Figure A.5.).

For needles, the onset of elongation occurred later in 2016 (late June) than in 2017 (early June). A 15% longer needle was formed in 2016. The highest shoot and needle growth rates took place in plot 1, whilst the smallest rates were observed in plot 4.

3.4. Needle and sapwood non-structural carbohydrate (NSC) concentrations

Sapwood SS and starch concentrations peaked in October, whereas needle SS concentrations peaked in August or before (April, June). Needle starch concentrations peaked in June (plots 1 and 2), April (plot 3) or October (plot 4). In 2016, maximum NSC concentrations in needles were reached in April in plot 4, June in plot 2 and August in plots 1 and 3 (Table 3). In sapwood, maximum TNC were reached in all plots in October. There was no significant difference in needle and sapwood NSC concentrations among plots.

Table 3. Average needle and sapwood concentrations (%) as soluble sugars (SS), starch and total non-structural carbohydrates (TNC) during 2016.

	Plot	Needles				Sapwood			
		April	June	August	October	April	June	August	October
SS	1	5.6	6.7	5.4	4.8	0.7	0.7	0.6	1.4
	2	4.6	7.6	10.5	7.2	3.9	4.0	3.9	5.6
	3	10.2	14.2	15.8	12.0	4.6	4.7	4.6	6.9
	4	5.4	4.6	3.9	4.2	0.5	0.7	0.7	1.0
Starch	1	14.1	20.4	6.7	7.9	3.4	3.9	3.7	4.8
	2	19.5	25.0	10.6	12.1	3.9	4.6	4.4	5.8
	3	5.5	4.6	5.2	4.8	0.6	0.6	0.8	1.1
	4	8.9	5.4	9.9	4.9	3.0	3.5	3.4	4.3
TNC	1	14.3	10.0	15.2	9.7	3.6	4.1	4.2	5.5
	2	5.9	4.7	7.0	4.2	1.5	0.8	1.1	1.2
	3	9.3	6.9	5.5	6.4	4.3	4.7	4.4	5.2

4	15.2	11.6	12.5	10.6	5.8	5.5	5.4	6.4

485 **Table 4.** Growth characteristics considering stem radius increment and production of mature tracheids. Average values during
486 2016, 2017 and 2018 at each plot are shown.

		Stem radius increment						Mature tracheids					
Year	Plot	Total radial increment ($mm \cdot y^{-1}$)	Onset (DOY)	Cessation (DOY)	Duration (days)	Max rate ($\mu m \cdot d^{-1}$)	Timing of max rate (DOY)	Cell production (Nº mature trach·y^{-1})	Onset (DOY)	Cessation (DOY)	Duration (days)	Max rate (nº mat trach·d^{-1})	Timing of max rate (DOY)
2016	1	0.26	159	191	32	10	171	30	163	297	134	0.23	221
	2	0.46	153	185	32	24	163	25	162	285	123	0.28	201
	3	0.57	143	199	56	15	162	70	162	302	140	0.62	222
	4	1.99	123	247	124	28	163	90	172	305	133	0.89	228
2017	1	0.49	125	189	64	9	149	21	161	246	85	0.42	182
	2	0.74	131	189	58	21	150	32	155	282	127	0.41	190
	3	0.81	120	210	90	12	153	35	151	272	121	0.76	172
	4	2.04	116	242	126	29	157	78	153	298	145	0.97	197
2018	1	0.69	132	235	103	6	173	–	–	–	–	–	–
	2	0.91	115	221	106	11	154	–	–	–	–	–	–
	3	0.94	123	245	122	9	169	–	–	–	–	–	–
	4	2.50	114	295	181	23	174	–	–	–	–	–	–

3.5. Microclimate influences on growth

Soil temperature was the microclimate variable most related to xylogenesis during June (when the first mature tracheids were observed) and September (during the final phase of tracheid maturation) (Figure 4a). The positive influence of soil temperature on growth mainly occurred throughout the entire spring. Soil temperatures (7-day mean) were 10.4 ± 1.4 ºC and 7.9 ± 2.8 ºC when the first and last mature tracheids were formed, respectively. A later soil warming onset can delay and therefore shorten the growing season, and this was related to a lower growth rate (see Figure A.6.). This was observed in 3 out of the 4 studied plots, with plot 4 not showing this relationship. Air temperature showed positive correlations to xylem development rates in May, when the first radially enlarging tracheids were detected. Air and soil temperatures (7-day mean) were 6.1 ± 3.1 ºC and 5.6 ± 3.6 ºC, respectively, when the first radially enlarging tracheids were observed. Mostly negative correlations of xylem development rates with soil VWC were found during September and during the spring in plot 4. An exception was the positive correlation found in plot 1 with April soil VWC.

For radial increment rates, air temperature was the variable that most related to these rates during May in all plots (Figure 4b). In most plots, soil temperatures were also relevant to the onset of stem radial increment. Air and soil temperatures (7-day means) were 8.4 ± 4.5 ºC and 5.9 ± 4.7 ºC respectively, when the stem radial increment began. July air H and July-August soil VWC were positively correlated to stem radial increment rates in all plots. Maximum radial increment rates occurred about 10 days earlier (± 9 days) than maximum day length.

509 The first principal component (PC1) of the first PCA explained 55.3% of the
510 variability (Table A.3.). Air T, soil T and xylem development rates spread along the PC1
511 axis increasing in same direction, while soil VWC increased in the opposite direction.
512 Rates of production of mature tracheids were highly and positively related to soil
513 temperature, followed by air temperature (Figure 5a). As air H spread along the second
514 principal component (PC2), explaining only a small percentage of variability (18.16 %),
515 its influence on formation of mature tracheids was low. The PC1 of the second PCA,
516 performed considering all microclimate variables and radial increment rates, explained
517 49.9% of the variability. All microclimate variables spread along the PC1 axis, where air
518 and soil T increased in the opposite direction of air H and soil VWC (Table A.3.). Radial
519 increment rates spread alone along the PC2 axis (22.1 %). Among microclimate
520 variables, soil VWC was related to radial increment rates (Figure 5b), followed by air H.

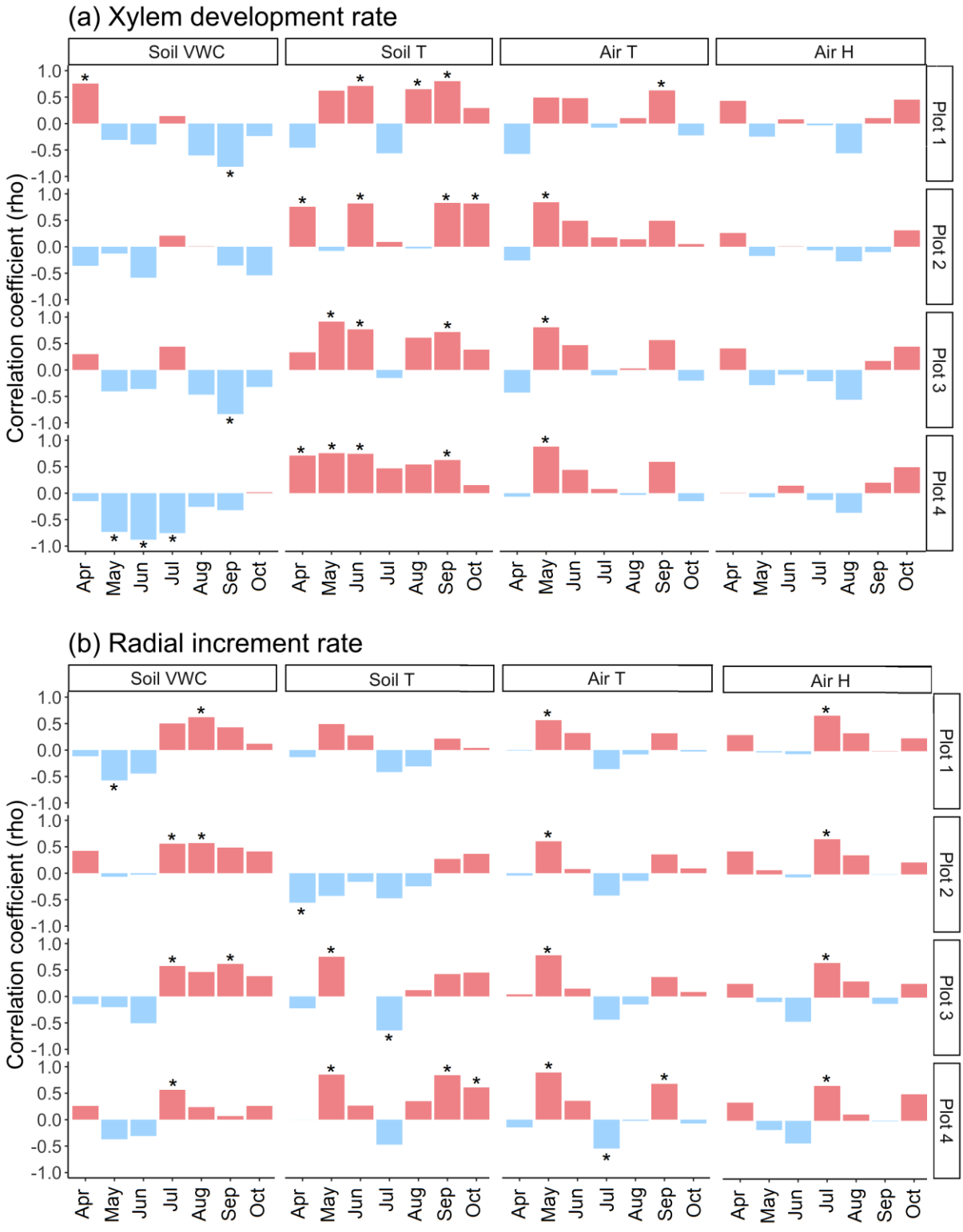

Figure 4. Spearman rho correlation coefficients calculated by month and plot between microclimate variables (weekly averages) and tree growth rates data series (weekly maximum values) of *P. uncinata* during the main growing period. (a) Xylem development rates corresponding to the production of mature tracheids comprised two years (2016, 2017) and (b) radial increment rates series comprised three years (2016, 2017, 2018). Therefore, the number of samples varied among correlations; as a

consequence, critical values for Spearman coefficients varied too. Asterisks highlight significant correlations ($p < 0.05$).

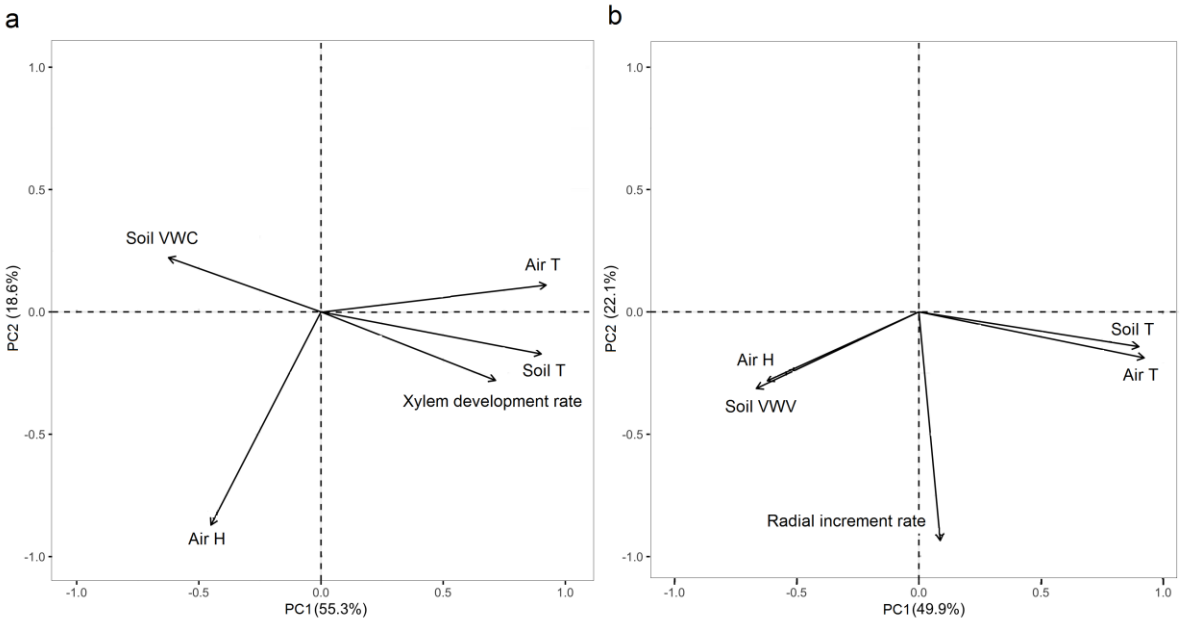

Figure 5. Principal component analysis of microclimate variables (weekly averages) and *P. uncinata* tree growth rates (weekly maximum values) during the main growing period. (a) Xylem development rates series corresponding to the production of mature tracheids comprised two years (2016, 2017) and (b) radial increment rates series comprised three years (2016, 2017 and 2018).

4. Discussion

Evidence has been presented to show how snow dynamics influence seasonal growth dynamics by influencing soil temperature in mountain forests. Soil temperature was the microclimate variable most relevant to the production of mature tracheids, highly influencing timing (onset and cessation) and resulting growth rates. As snowpack duration determines soil warming at the beginning of the growing season, a larger and more lasting snowpack induces a retarded cambial reactivation and is related to lower growth rates. Hence, this study at intra-annual scale, confirms what Sanmiguel-Vallelado et al. (2019) found at inter-annual scale in a tree-ring network of *P. uncinata* forests. The

548 results provide additional information about the effects of climate and soil temperature
549 and humidity conditions on radial growth

550 The winter snow accumulation, the time of melt-out date, the onset of the growing
551 season and the growth rates were strongly interrelated (Helama et al., 2013; Kirdyanov
552 et al., 2003). In this study it was observed that larger snow accumulation involved later
553 snow depletion that, in connection with lower spring air temperatures, produced a delay
554 in soil warming onset and in tracheid maturation. Therefore, the most limiting factor to
555 xylem development found in this study was low soil temperature in June. On the one
556 hand, the soil cooling induced by snow presence can be explained by the effects of high
557 snow albedo and high latent heat due to snowmelt is a heat sink (Zhang, 2005). On the
558 other hand, low soil temperatures had been reported to inhibit root activity (Alvarez-
559 Uria and Körner, 2007), which could explain an indirect effect on cambium reactivation
560 in the spring, since roots provide water and nutrients to meristems such as the
561 cambium. Several potential physiological mechanisms by which cool soils may limit
562 conifer growth have been described in the literature. Kozlowski (1964) suggested that trees
563 cannot uptake water through their roots and initiate hydraulic and metabolic processes until
564 snowpacks wane to a threshold at which soil temperatures increase and viscosity decreases.
565 CO_2 uptake was decreased at low root temperatures and appeared to be influenced by the
566 pattern of nitrogen translocation (Vapaavuori et al., 1992). In cold substrates (< 5 °C), root
567 growth in *P. sylvestris* has been found to be constrained by plasma membrane H+-ATPase
568 (PM-ATPase) transport, which has multiple functions in cell growth (Iivonen et al., 1999).
569 Furthermore, Peterson and Peterson (2001) suggest that increased cloudiness, associated with

570 cool springs and late-lying snowpacks, could reduce solar radiation and increase the
571 frequency of photoinhibition following cold nights.

572 The highest correlation between air temperature and xylem development rates in
573 most plots was found when the first radially enlarging tracheids were formed. By this
574 time, the observed mean air temperature (6ºC) is similar to the 5°C minimal air
575 temperature threshold proposed by Rossi et al. (2008) for conifers from cold sites.
576 Previous tree-ring studies demonstrated that low air temperatures during the growing
577 season limit growth of *P. uncinata* (Andreu et al., 2007; Camarero et al., 1998; Galván et
578 al., 2014; Rolland and Schueller, 1994; Tardif et al., 2003). Nevertheless, due to the
579 stronger coupling between mature tracheids and soil temperature observed in this
580 study, we argue that 10ºC soil temperature when first mature tracheids were developed
581 should be also considered.

582 Tracheid maturation onset always occurred after complete melt-out. In most cases,
583 it was observed that a later tracheid maturation leads to a shorter growing season and,
584 therefore, limits growth and wood production (Lenz et al., 2013). The observed
585 reduction in growth rates induced by snow-related cold soil temperatures is more
586 relevant to wood production than growing season duration (Cuny et al., 2015). Apart
587 from that, low soil temperatures in September reduced xylem development; therefore,
588 the soil cooling in early autumn seems also to affect the last phases of xylogenesis (Cuny
589 et al., 2014). These results agree with the negative influences that Sanmiguel-Vallelado
590 et al. (2019) found between winter snow accumulation and late spring snow presence
591 on *P. uncinata* growth and provide an in-depth explanation at a finer temporal
592 resolution.

593 Although the highest NSC concentration in sapwood was found in the coldest plot,
594 no difference in NSC concentration was found among plots along the altitudinal gradient,
595 and there was no link with growth dynamics. Similarly, Gruber et al. (2011) did not find
596 evidence that an insufficient carbon balance limits growth at their upper elevational
597 limit. This confirms that radial growth and the storage and mobilization of carbon pools
598 are not necessarily coupled (Körner, 2012). The needle starch concentration was
599 observed when needles started elongating during June in some plots (e.g. plot 2), and
600 this was followed by a peak in SS concentration in August, suggesting the differential use
601 of these NSCs to build the new foliage. Since highest NSC concentration in sapwood
602 occurred in October, when xylogenesis finished, the observed dynamics of sapwood NSC
603 did not follow xylogenesis, whereas in other studies they were more coupled to
604 latewood formation (Oberhuber et al., 2011).

605 The onset of stem radial increment in *P. uncinata* (DOY 130 ± 15), occurred on
606 average 15 days in advance of the onset of mature tracheid formation, probably
607 reflected the date when stem re-hydration started (Zweifel et al., 2000). We observed a
608 value of 6 ºC in 7-day average soil temperature for the onset of stem radial increment,
609 which agrees with the fact that soil temperatures lower than 6ºC inhibit water uptake by
610 roots in several conifers (Alvarez-Uria and Körner, 2007). As water from snow melting
611 infiltrates into the soil during winter, it is available for trees even before the complete
612 snow depletion, once the soil starts warming and triggers fine root activity. Warmer air
613 temperatures in May – we observed a value of 8 ºC in 7-day average air temperature for
614 the onset of stem radial increment – promoted stem radial increment rates in the study
615 area, may be because they facilitated water release from snow – we observed an
616 important water contribution to soil moisture from snowmelt in that time – and

617 stimulated cambium resumption (Camarero et al., 1998) Radial increment rates were
618 mainly driven by soil moisture and air humidity, reflecting the strong linkage between
619 stem radial fluctuations and changes in tree water status even in high-elevation forests
620 (Zweifel et al., 2000). However, only a positive influence of early spring snowmelt on
621 xylem development was observed in plot 1, where the lowest soil moisture values are
622 found. Therefore, we cannot demonstrate that snowmelt water promoted *P. uncinata*
623 growth in the study site. Similarly, Turcotte et al. (2009) reported that growth initiation
624 in black spruce was not limited by the spring rehydration. This soil moisture limitation
625 was reported in more arid mountain ranges (St. George, 2014). The cessation of the stem
626 radial increment period and the start of latewood formation are triggered by warm-dry
627 air and soil conditions in summer.

628 We found no clear microclimate influences on maximum rates of production of
629 mature tracheids or radial increment, neither in terms of timing nor in magnitude. It has
630 been reported that the maximum growth rates of conifers from cold sites synchronized
631 with the longest day in the year (Rossi et al., 2006). Our observations agree with this
632 idea since stem radial maximum rates occurred around 10 days earlier than the summer
633 solstice.

634 We also observed a high variability in small spatial scale in microclimate
635 conditions and also in tree growth and NSCs. All plots showed similar snow influences
636 on seasonal growth dynamics, with some variation in strength; however, when
637 considering annual snow-growth effects and the inter-plot variability, plot 4 stepped out
638 of line. This plot (the coldest site situated at highest elevation and with a northern
639 aspect) showed the longest growing season and largest growth rates despite the

640 presence of the longest-lasting snowpacks, contrary to what was expected. This
641 behavior in plot 4 could be explained by high solar radiation values in spring. In
642 addition, more water availability, and for longer periods, may prevent *P. uncinata* from
643 drought, in contrast to what can occur when water is scarce during summer in shallow
644 and rocky soils (Galván et al., 2014). However, more research will be needed to
645 determine which ultimate factors determine the differences between plots. Therefore, *P.*
646 *uncinata* growth was determined, to a large extent, by snow dynamics in 3 out of the 4
647 studied plots. Excepting plot 4, a later snow melt-out date delayed and shortened the *P.*
648 *uncinata* growing season, thus reducing growth. Rossi et al. (2011) previously confirmed
649 that delayed snowmelt reduced growth in boreal forests of *Picea mariana* in Quebec,
650 Canada. Previously, Vaganov et al. (1999) found that in the Russian taiga conifers
651 showed a lower growth when snow melt was delayed in the early growing season. This
652 study extends these observations to high-elevation mountain forests of mid-latitude
653 ranges such as the Pyrenees, and highlights the need to consider the small-scale
654 variability of microclimate effects on individual tree growth of mountain forests.

655 The abovementioned inter-plot variability in microclimate conditions and tree
656 growth was much larger than inter-annual variability in most cases. Inter-annual
657 variability in growth dynamics may be induced by microclimate conditions, at least in a
658 part. For example, in 2016, the warmest air and soil temperatures observed during the
659 TGS might promote the highest production of mature tracheids. All our four sites are
660 mainly characterized by temperature limitation of growth, as we have discussed
661 previously. Therefore, low temperatures during the growing season limit the tree
662 growth (Rossi et al., 2008). In 2017, the earliest melt-out dates might lead to the earliest
663 starting and peaking date of mature tracheids production. We previously mentioned

664 that the energy-limited influence of snow on studied forest, due to long-lasting
665 snowpacks, could be an appropriate explanation for the positive influence of soil
666 temperature on tree growth found in this study (Helama et al., 2013; Kirdyanov et al.,
667 2003). In 2018, the highest radial growth observed might reflect the largest soil
668 moisture conditions during the growing season. As previously stated, we found
669 evidence that stem radial fluctuations were strongly related to tree hydrous state in the
670 studied forests (Zweifel et al., 2000).Under the current climate warming context,
671 increasing trends in air temperature had been already reported in the Spanish Pyrenees
672 (El Kenawy et al., 2011). Future warmer air and soil temperatures are expected to
673 prolong the *P. uncinata* growing season, and therefore, to enhance growth of Pyrenean
674 high-elevation forests and treelines during the late 21st century (Camarero et al., 2017;
675 Sánchez-Salguero et al., 2012). An increase in precipitation variability has been also
676 reported in this mountain range (López-Moreno et al., 2010). Therefore, these forecasts
677 could be amplified if climate change also affects snow dynamics (accumulation, duration
678 and melting) leading to shallower snowpacks and a longer snow-free period (Alonso-
679 González et al., 2020; Morán-Tejeda et al., 2017; López-Moreno et al., 2017). Overall,
680 growth of high-elevation *P. uncinata* novel forests could be benefited from the projected
681 future snow and air temperature projections. This positive effect could be explained by a
682 longer growing season, and a subsequently enhanced growth rate due to an earlier rise
683 and a later cooling of soil temperatures. Faster growth rates are related to shorter tree
684 longevity, and it is expected to lead to a reduced capacity of old forest ecosystems to
685 store carbon under warmer future (Büntgen et al., 2019), but new young forests could
686 also represent relevant carbon pools.

687

5. Conclusions

The seasonal growth dynamics of high-elevation *P. uncinata* forests were affected by snow dynamics. Soil temperature was the most relevant microclimate variable during the overall xylogenesis, mainly influencing the production of mature tracheids. Larger snow accumulation involved later snow depletion that produced a delay in soil warming onset. Low soil temperatures in spring, due to prolonged snow persistence, retarded the cambial onset and reduced growth rates. Wood production was affected by snow dynamics in three out of the four studied plots through a delayed and shorter growing season. This study highlights the large role of early and late growing season soil temperatures on radial growth, in addition to the widely reported effect of air temperature. A future shallower and more ephemeral snowpack in similar mountain, young forests, together with warmer air and soil temperatures, may enhance productivity and tree growth by prolonging the growing season through an earlier onset and a late cessation of xylogenesis.

Acknowledgements

We sincerely thank colleagues, friends and relatives who helped during the field surveys.

Funding

This study was supported by the projects: "*Bosque, nieve y recursos hídricos en el Pirineo ante el cambio global*" funded by Fundación Iberdrola, CGL2014-52599-P (IBERNIEVE) and CGL2017-82216-R (HIDROIBERNIEVE) funded by the Spanish Ministry of Economy

711 and Competitiveness. ASV was supported by a pre-doctoral University Professor
712 Training grant [FPU16/00902] funded by the Spanish Ministry of Education, Culture and
713 Sports. EAG was supported by a pre-doctoral FPI grant [BES-2015-071466] funded by
714 the Spanish Ministry of Economy and Competitiveness. JJC, AG and MC acknowledge
715 funding by project RTI2018-096884-B-C31 (Spanish Ministry of Economy and
716 Competitiveness).

References

Albrich, K., Rammer, W., Seidl, R., 2020. Climate change causes critical transitions and irreversible alterations of mountain forests. Glob. Change Biol. n/a. https://doi.org/10.1111/gcb.15118

Alonso-González, E., López-Moreno, J.I., Navarro-Serrano, F., Sanmiguel-Vallelado, A., Aznárez-Balta, M., Revuelto, J., Ceballos, A., 2020. Snowpack Sensitivity to Temperature, Precipitation, and Solar Radiation Variability over an Elevational Gradient in the Iberian Mountains. Atmos. Res. 243, 104973. https://doi.org/10.1016/j.atmosres.2020.104973.

Alvarez-Uria, P., Körner, C., 2007. Low temperature limits of root growth in deciduous and evergreen temperate tree species. Funct. Ecol. 21, 211 – 218. https://doi.org/10.1111/j.1365-2435.2007.01231.x

Andreu, L., Gutiérrez, E., Macias, M., Ribas, M., Bosch, O., Camarero, J.J., 2007. Climate increases regional tree-growth variability in Iberian pine forests. Glob. Change Biol. 13, 804–815.

Antonova, G.F., Stasova, V. V., 1993. Effects of environmental factors on wood formation in Scots pine stems. Trees, 7(4), 214-219. https://doi.org/10.1007/BF00202076

Babst, F., Bouriaud, O., Poulter, B., Trouet, V., Girardin, M.P., Frank, D.C., 2019. Twentieth century redistribution in climatic drivers of global tree growth. Sci. Adv., 5: eaat4313.

Barnett, T.P., Adam, J.C., Lettenmaier, D.P., 2005. Potential impacts of a warming climate on water availability in snow-dominated regions. Nature, 438(7066), 303–309. https://doi.org/10.1038/nature04141

Beniston, M., 2012. Is snow in the Alps receding or disappearing? Wiley Interdiscip. Rev. Clim. Change 3, 349–358.

Breiman, L., 2001. Random forests. Mach. Learn. 45, 5–32.

Büntgen, U., Krusic, P.J., Piermattei, A., Coomes, D.A., Esper, J., Myglan, V.S., Kirdyanov, A.V., Camarero, J.J., Crivellaro, A., Körner, C., 2019. Limited capacity of tree growth to

mitigate the global greenhouse effect under predicted warming. Nat. Commun. 10, 2171. https://doi.org/10.1038/s41467-019-10174-4.

Camarero, J.J., Guerrero-Campo, J., Gutierrez, E., 1998. Tree-Ring Growth and Structure of Pinus uncinata and Pinus sylvestris in the Central Spanish Pyrenees. Arct. Alp. Res. 30, 1. https://doi.org/10.2307/1551739

Camarero, J.J., Linares, J.C., García-Cervigón, A.I., Batllori, E., Martínez, I., Gutiérrez, E., 2017. Back to the future: the responses of alpine treelines to climate warming are constrained by the current ecotone structure. Ecosystems 20, 683–700.

Camarero, J.J., Olano, J.M., Parras, A., 2010. Plastic bimodal xylogenesis in conifers from continental Mediterranean climates. New Phytol. 185, 471–480. https://doi.org/10.1111/j.1469-8137.2009.03073.x

Cantegrel, R., 1983. Le Pin à crochets pyrénéen: biologie, biochimie, sylviculture. Acta Biol. Mont. 2, 87–330.

Carlson, K.M., Coulthard, B., Starzomski, B.M., 2017. Autumn snowfall controls the annual radial growth of centenarian whitebark pine (*Pinus albicaulis*) in the southern Coast Mountains, British Columbia, Canada. Arct. Antarct. Alp. Res. 49, 101–113.

Cuny, H.E., Rathgeber, C.B.K., Frank, D., Fonti, P., Fournier, M., 2014. Kinetics of tracheid development explain conifer tree-ring structure. New Phytol. 203, 1231–1241. https://doi.org/10.1111/nph.12871

Cuny, H.E., Rathgeber, C.B.K., Frank, D., Fonti, P., Mäkinen, H., Prislan, P., Rossi, S., del Castillo, E.M., Campelo, F., Vavrčík, H., Camarero, J.J., Bryukhanova, M.V., Jyske, T., Gričar, J., Gryc, V., De Luis, M., Vieira, J., Čufar, K., Kirdyanov, A.V., Oberhuber, W., Treml, V., Huang, J.-G., Li, X., Swidrak, I., Deslauriers, A., Liang, E., Nöjd, P., Gruber, A., Nabais, C., Morin, H., Krause, C., King, G., Fournier, M., 2015. Woody biomass production lags stem-girth increase by over one month in coniferous forests. Nature Plants 1, 15160. https://doi.org/10.1038/nplants.2015.160

D'Orangeville, L., Côté, B., Houle, D., Morin, H., Duchesne, L., 2013. A three-year increase in soil temperature and atmospheric N deposition has minor effects on the

774 xylogenesis of mature balsam fir. Trees 27, 1525–1536.
775 https://doi.org/10.1007/s00468-013-0899-4

776 Dan Moore, R., Spittlehouse, D., Story, A., 2005. Riparian microclimate and stream
777 temperature response to forest harvesting: a review. Am. Water Resour. Assoc. 41,
778 813–834.

779 Del Barrio, G., Creus, J., Puigdefábregas, J., 1990. Thermal seasonality of the high
780 mountain belts of the Pyrenees. Mt. Res. Dev. 227–233.

781 Denne, M.P., 1989. Definition of Latewood According to Mork (1928). Am. Water Resour.
782 Assoc. 10, 59–62. https://doi.org/10.1163/22941932-90001112

783 Deslauriers, A., Rossi, S., Anfodillo, T., 2007. Dendrometer and intra-annual tree growth:
784 What kind of information can be inferred? Dendrochronologia 25, 113–124.
785 https://doi.org/10.1016/j.dendro.2007.05.003

786 Deslauriers, A., Rossi, S., Liang, E., 2015. Collecting and Processing Wood Microcores for
787 Monitoring Xylogenesis, in: Yeung, E.C.T., Stasolla, C., Sumner, M.J., Huang, B.Q.
788 (Eds.), Plant Microtechniques and Protocols. Springer International Publishing,
789 Cham, pp. 417–429. https://doi.org/10.1007/978-3-319-19944-3_23

790 El Kenawy, A., López-Moreno, J.I., Vicente-Serrano, S.M., 2011. Recent trends in daily
791 temperature extremes over northeastern Spain (1960–2006). Nat. Hazards Earth
792 Syst. Sci. 11, 2583–2603. https://doi.org/10.5194/nhess-11-2583-2011

793 Galván, J.D., Camarero, J.J., Gutiérrez, E., 2014. Seeing the trees for the forest: drivers of
794 individual growth responses to climate in *Pinus uncinata* mountain forests. J. Ecol.
795 102, 1244–1257.

796 Gruber, A., Pirkebner, D., Oberhuber, W., Wieser, G., 2011. Spatial and seasonal
797 variations in mobile carbohydrates in *Pinus cembra* in the timberline ecotone of the
798 Central Austrian Alps. Eur. J. For. Res. 130, 173–179.
799 https://doi.org/10.1007/s10342-010-0419-7

800 Harpold, A.A., Molotch, N.P., Musselman, K.N., Bales, R.C., Kirchner, P.B., Litvak, M.,
801 Brooks, P.D., 2015. Soil moisture response to snowmelt timing in mixed-conifer

802 subalpine forests: Hydrol. Process. 29, 2782–2798.
803 https://doi.org/10.1002/hyp.10400

804 Helama, S., Mielikainen, K., Timonen, M., Herva, H., Tuomenvirta, H., Venalainen, A., 2013.
805 Regional climatic signals in Scots pine growth with insights into snow and soil
806 associations. Dendrobiology 70.

807 Iivonen, S., Rikala, R., Ryyppö, A., Vapaavuori, E., 1999. Responses of Scots pine (Pinus
808 sylvestris) seedlings grown in different nutrient regimes to changing root zone
809 temperature in spring. Tree Physiology 19, 951–958.

810 Jolliffe, I.T., 2012. Choosing a Subset of principal Components or Variables. In: Principal
811 Coponent Analysis. Springer Series in Statistics. Springer, New York, NY.
812 https://doi.org/10.1007/0-387-22440-8_6

813 Kaiser, H.F., 1974. An index of factorial simplicity. Psychometrika 39, 31-36.

814 Kirdyanov, A., Hughes, M., Vaganov, E., Schweingruber, F., Silkin, P., 2003. The
815 importance of early summer temperature and date of snow melt for tree growth in
816 the Siberian Subarctic. Trees 17, 61–69.

817 Körner, C., 2012. Alpine treelines: functional ecology of the global high elevation tree
818 limits. Springer Science & Business Media.

819 Kozlowski, T.T., 1964. Water Metabolism in Plants. Soil Science 98, 143.

820 Lenz, A., Hoch, G., Körner, C., 2013. Early season temperature controls cambial activity
821 and total tree ring width at the alpine treeline. Plant Ecol. Divers. 6, 365–375.
822 https://doi.org/10.1080/17550874.2012.711864

823 López-Moreno, J.I., Gascoin, S., Herrero, J., Sproles, E.A., Pons, M., Alonso-González, E.,
824 Hanich, L., Boudhar, A., Musselman, K.N., Molotch, N.P., Sickman, J., Pomeroy, J.,
825 2017. Different sensitivities of snowpacks to warming in Mediterranean climate
826 mountain areas. Environ. Res. Lett. 12(7), 074006.

827 López-Moreno, J.I., Vicente-Serrano, S.M., Angulo-Martínez, M., Beguería, S., Kenawy, A.,
828 2010. Trends in daily precipitation on the northeastern Iberian Peninsula, 1955–
829 2006. Int. J. Climatol. 30, 1026–1041.

Lupi, C., Morin, H., Deslauriers, A., Rossi, S., 2012. Xylogenesis in black spruce: does soil temperature matter? Tree Physiol. 32, 74–82. https://doi.org/10.1093/treephys/tpr132

McCabe, G.J., Wolock, D.M., 2009. Recent declines in western US snowpack in the context of twentieth-century climate variability. Earth Interact. 13, 1–15.

Morán-Tejeda, E., López-Moreno, J.I., Sanmiguel-Vallelado, A., 2017. Changes in climate, snow and water resources in the Spanish Pyrenees: observations and projections in a warming climate, in: High Mountain Conservation in a Changing World. Springer, pp. 305–323.

Oberhuber, W., Swidrak, I., Pirkebner, D., Gruber, A., 2011. Temporal dynamics of non-structural carbohydrates and xylem growth in Pinus sylvestris exposed to drought. Can. J. For. Res. 41, 1590–1597. https://doi.org/10.1139/x11-085

Palacio, S., Maestro, M., Montserratmarti, G., 2007. Seasonal dynamics of non-structural carbohydrates in two species of mediterranean sub-shrubs with different leaf phenology. Env. Exp. Bot. 59, 34–42. https://doi.org/10.1016/j.envexpbot.2005.10.003

Pederson, G.T., Gray, S.T., Woodhouse, C.A., Betancourt, J.L., Fagre, D.B., Littell, J.S., Watson, E., Luckman, B.H., Graumlich, L.J., 2011. The unusual nature of recent snowpack declines in the North American Cordillera. Science 333, 332–335. https://doi.org/10.1126/science.1201570

Peterson, D.W., Peterson, D.L., 2001. Mountain Hemlock Growth Responds to Climatic Variability at Annual and Decadal Time Scales. Ecology 82, 3330–3345. https://doi.org/10.1890/0012-9658(2001)082[3330:MHGRTC]2.0.CO;2

R Core Team, 2018. R Foundation for Statistical Computing; Vienna, Austria: 2015. R Lang. Environ. Stat. Comput. 2013.

Rasband, W.S., 1997. ImageJ. US National Institutes of Health, Bethesda, MD, USA. http://rsb.info.nih.gov/ij/

Rodriguez Perez, D., 2013. growthmodels: Nonlinear Growth Models. R package version 1.2.0. https://CRAN.R-project.org/package=growthmodels

859 Rolland, C., Schueller, J.F., 1994. Relationships between mountain pine and climate in the
860 French Pyrenees (Font-Romeu) studied using the radiodensitometrical method.
861 Pirineos 143, 55–70.

862 Rossi, S., Deslauriers, A., Anfodillo, T., Carraro, V., 2007. Evidence of threshold
863 temperatures for xylogenesis in conifers at high altitudes. Oecologia 152, 1–12.
864 https://doi.org/10.1007/s00442-006-0625-7

865 Rossi, S., Deslauriers, A., Anfodillo, T., Morin, H., Saracino, A., Motta, R., Borghetti, M.,
866 2006. Conifers in cold environments synchronize maximum growth rate of tree-ring
867 formation with day length. New Phytol. 170, 301–310.
868 https://doi.org/10.1111/j.1469-8137.2006.01660.x

869 Rossi, S., Deslauriers, A., Griçar, J., Seo, J.W., Rathgeber, C.B., Anfodillo, T., Morin, H.,
870 Levanic, T., Oven, P., Jalkanen, R., 2008. Critical temperatures for xylogenesis in
871 conifers of cold climates. Glob. Ecol. Biogeogr. 17, 696–707.
872 https://doi.org/10.1111/j.1466-8238.2008.00417.x

873 Rossi, S., Deslauriers, A., Morin, H., 2003. Application of the Gompertz equation for the
874 study of xylem cell development. Dendrochronologia 21, 33–39.
875 https://doi.org/10.1078/1125-7865-00034

876 Rossi, S., Morin, H., Deslauriers, A., 2011. Multi-scale Influence of snowmelt on
877 xylogenesis of Black Spruce. Arct. Antarct. Alp. Res. 43, 457–464.
878 https://doi.org/10.1657/1938-4246-43.3.457

879 Rossi, S., Rathgeber, C.B.K., Deslauriers, A., 2009. Comparing needle and shoot phenology
880 with xylem development on three conifer species in Italy. Ann. For. Sci. 66, 206–206.
881 https://doi.org/10.1051/forest/2008088

882 Ruiz de la Torre, J., Ceballos, L., 1979. Arboles y Arbustos de la España Peninsular. ETSI
883 de Montes. Madrid. 512 pp. ISBN 84–600–84–600.

884 Sánchez-Salguero, R., Navarro-Cerrillo, R.M., Swetnam, T.W., Zavala, M.A., 2012. Is
885 drought the main decline factor at the rear edge of Europe? The case of southern
886 Iberian pine plantations. For. Ecol. Manag. 271, 158–169.

887 Sangüesa-Barreda, G., Linares, J.C., Camarero, J.J., 2012. Mistletoe effects on Scots pine
888 decline following drought events: insights from within-tree spatial patterns, growth
889 and carbohydrates. Tree Physiol. 32, 585–598.
890 https://doi.org/10.1093/treephys/tps031

891 Sanmiguel-Vallelado, A., Camarero, J.J., Gazol, A., Morán-Tejeda, E., Sangüesa-Barreda, G.,
892 Alonso-González, E., Gutiérrez, E., Alla, A.Q., Galván, J.D., López-Moreno, J.I., 2019.
893 Detecting snow-related signals in radial growth of Pinus uncinata mountain forests.
894 Dendrochronologia 57, 125622. https://doi.org/10.1016/j.dendro.2019.125622

895 Sanmiguel-Vallelado, A., López-Moreno, J.I., Morán-Tejeda, E., Alonso-González, E.,
896 Navarro-Serrano, F.M., Rico, I., Camarero, J.J., 2020. Variable effects of forest
897 canopies on snow processes in a valley of the central Spanish Pyrenees. Hydrol.
898 Process. hyp.13721. https://doi.org/10.1002/hyp.13721

899 St. George, S., 2014. An overview of tree-ring width records across the Northern
900 Hemisphere. Quat. Sci. Rev. 95, 132–150.
901 https://doi.org/10.1016/j.quascirev.2014.04.029

902 Stekhoven, D.J., Buhlmann, P., 2012. MissForest--non-parametric missing value
903 imputation for mixed-type data. Bioinformatics 28, 112–118.
904 https://doi.org/10.1093/bioinformatics/btr597

905 Tardif, J., Camarero, J.J., Ribas, M., Gutiérrez, E., 2003. Spatiotemporal variability in tree
906 growth in the Central Pyrenees: climatic and site influences. Ecol. Monogr. 73, 241–
907 257.

908 Truettner, C., Anderegg, W.R.L., Biondi, F., Koch, G.W., Ogle, K., Schwalm, C., Litvak, M.E.,
909 Shaw, J.D., Ziaco, E., 2018. Conifer radial growth response to recent seasonal
910 warming and drought from the southwestern USA. For. Ecol. Manag. 418, 55–62.
911 https://doi.org/10.1016/j.foreco.2018.01.044

912 Turcotte, A., Morin, H., Krause, C., Deslauriers, A., Thibeault-Martel, M., 2009. The timing
913 of spring rehydration and its relation with the onset of wood formation in black
914 spruce. Agricultural and Forest Meteorology 149, 1403–1409.
915 https://doi.org/10.1016/j.agrformet.2009.03.010

916 Vaganov, E.A., Hughes, M.K., Kirdyanov, A.V., Schweingruber, F.H., Silkin, P.P., 1999.
917 Influence of snowfall and melt timing on tree growth in subarctic Eurasia. Nature
918 400, 149–151. https://doi.org/10.1038/22087

919 van der Maaten, E., van der Maaten-Theunissen, M., Smiljanić, M., Rossi, S., Simard, S.,
920 Wilmking, M., Deslauriers, A., Fonti, P., von Arx, G., Bouriaud, O., 2016. dendrometeR:
921 Analyzing the pulse of trees in R. Dendrochronologia 40, 12–16.
922 https://doi.org/10.1016/j.dendro.2016.06.001

923 Vapaavuori, E.M., Rikala, R., Ryyppö, A., 1992. Effects of root temperature on growth and
924 photosynthesis in conifer seedlings during shoot elongation. Tree Physiology 10,
925 217–230.

926 Watson, E., Luckman, B.H., 2016. An investigation of the snowpack signal in moisture-
927 sensitive trees from the Southern Canadian Cordillera. Dendrochronologia 38, 118–
928 130. https://doi.org/10.1016/j.dendro.2016.03.008

929 Woelber, B., Maneta, M. P., Harper, J., Jencso, K. G., Gardner, W. P., Wilcox, A. C., López-
930 Moreno, I., 2018. The influence of diurnal snowmelt and transpiration on hillslope
931 throughflow and stream response. Hydrol. Earth Syst. Sc., 22(8).
932 https://doi.org/10.5194/hess-22-4295-2018

933 Zeide, B., 1993. Analysis of growth equations. For. Sci., 39:594–616.

934 Zhang, L., Axmacher, J.C., Sang, W., 2017. Different radial growth responses to climate
935 warming by two dominant tree species at their upper altitudinal limit on Changbai
936 Mountain. J. For. Res. 28, 795–804. https://doi.org/10.1007/s11676-016-0364-5

937 Zhang, T., 2005. Influence of the seasonal snow cover on the ground thermal regime: An
938 overview. Rev. Geophys. 43. https://doi.org/10.1029/2004RG000157

939 Zhang, X., Manzanedo, R.D., D'Orangeville, L., Rademacher, T.T., Li, J., Bai, X., Hou, M.,
940 Chen, Z., Zou, F., Song, F., Pederson, N., 2019. Snowmelt and early to mid-growing
941 season water availability augment tree growth during rapid warming in southern
942 Asian boreal forests. Glob. Change Biol. 25, 3462–3471.
943 https://doi.org/10.1111/gcb.14749

944 Zweifel, R., Item, H., Häsler, R., 2000. Stem radius changes and their relation to stored
945 water in stems of young Norway spruce trees. Trees 15, 50–57.
946 https://doi.org/10.1007/s004680000072

Appendices

Figure A.1. (a) Monitoring seasonality throughout 2016 as an example of one year of data collection, and (b) differences in variables acquired among years.

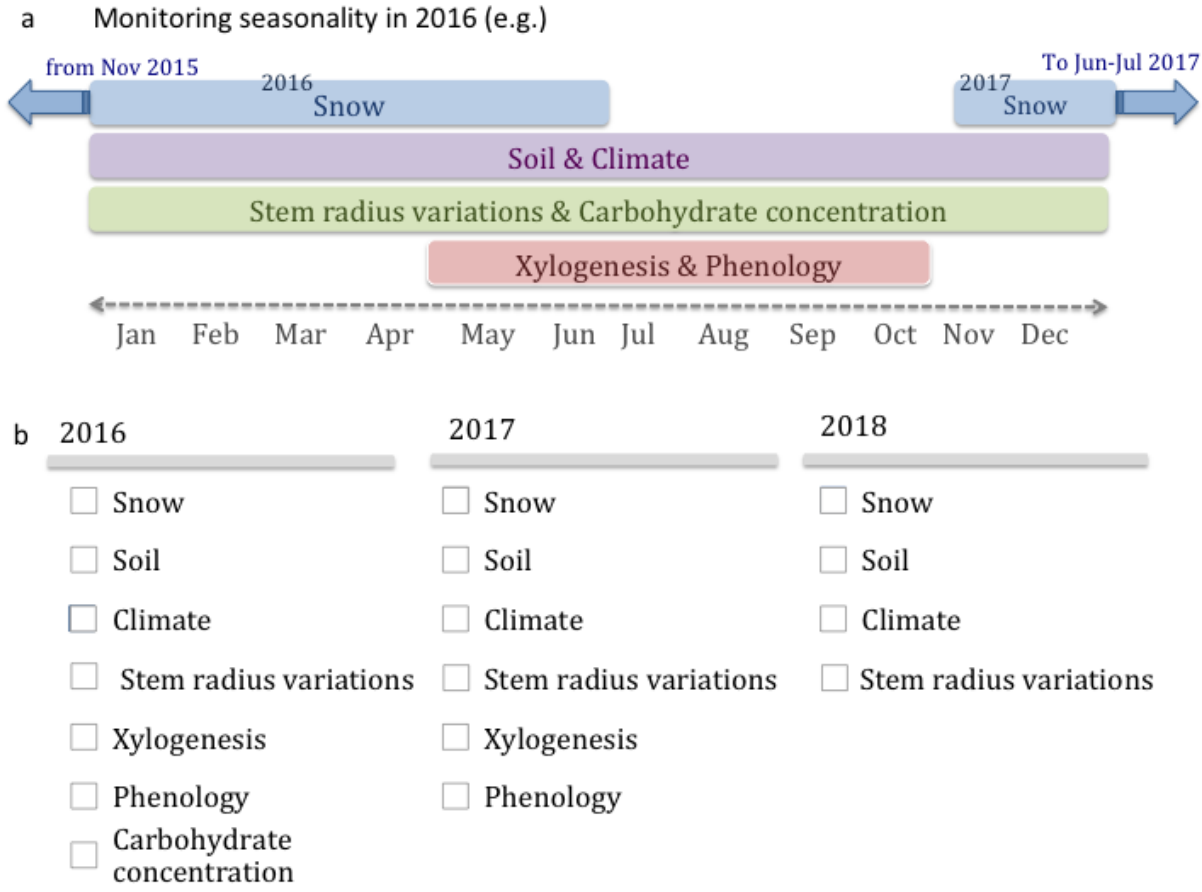

Figure A.2. Scatterplot of the relationships between (a) SWE peak and snowmelt out date and (b) between snow melt out date and soil warming onset. Pearson correlation coefficients between indices and *p* values are shown.

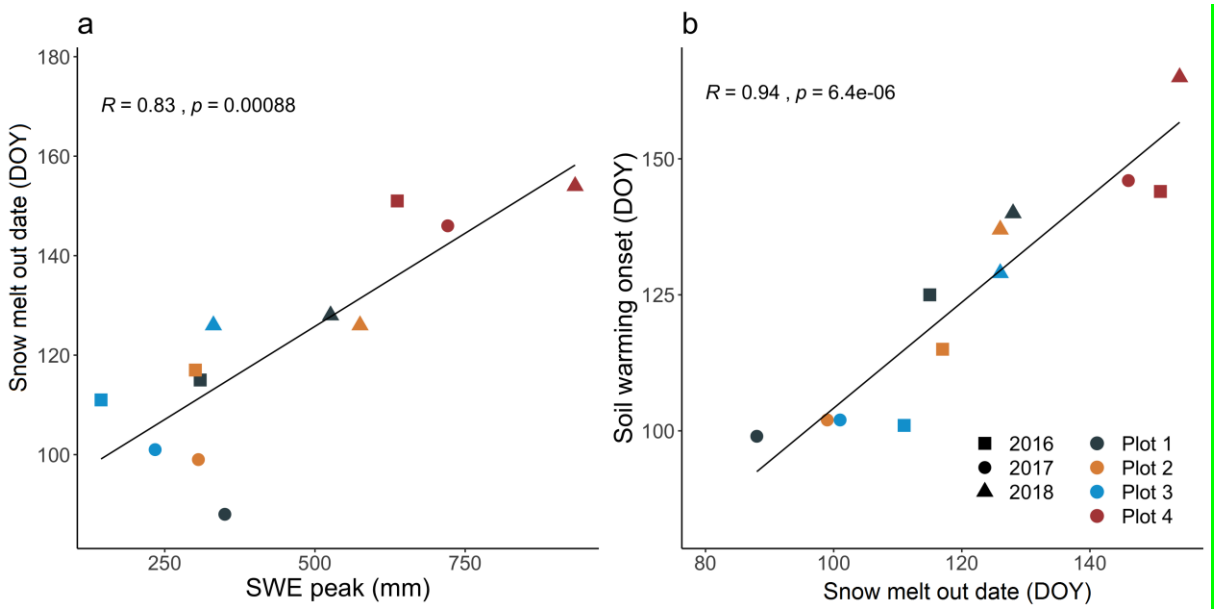

Figure A.3. (a) Polynomial regressions between monthly averages of SWE and soil temperature by plot for the four study plots considering data collected during 2016, 2017 and 2018. (b) Scatterplots of timing of melt-out date and May and June soil temperatures considering data collected during 2016, 2017 and 2018. Pearson correlation coefficients and *p* values are shown.

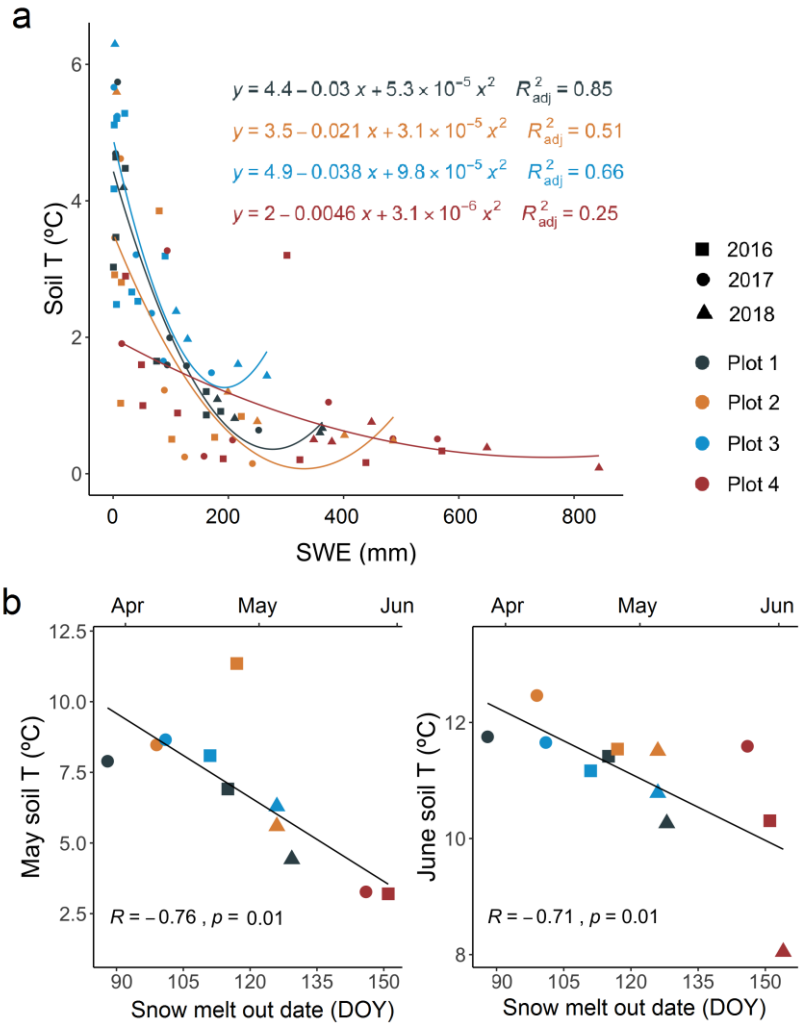

Figure A.4. (a) Linear regressions between monthly sums of snowmelt and monthly averages of soil VWC by plot considering data collected during 2016, 2017 and 2018 (b) Spearman correlation coefficients calculated by month and plot between snowmelt weekly sums and soil VWC weekly averages considering data collected during 2016, 2017 and 2018. Asterisks highlight significant correlations (p < 0.05). Note that the number of samples and significance levels varied among months and plots.

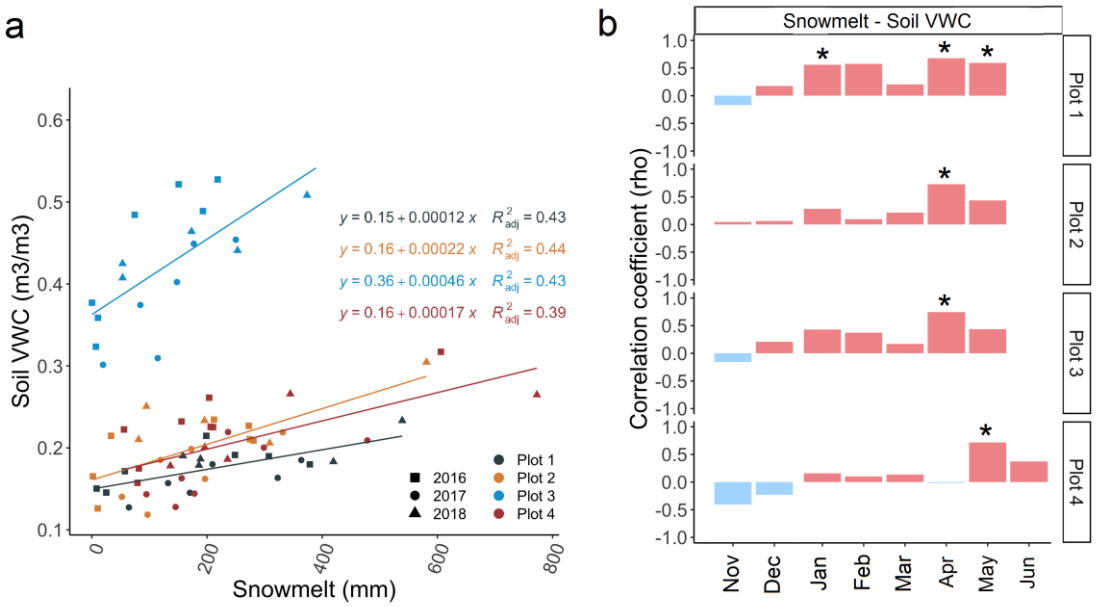

Figure A.5. Time series of needle (top panel) and shoot (bottom panel) length during the 2016 and 2017 growing seasons (dots: mean values; error bars: standard deviation). Timing is represented by the day of the natural year (DOY).

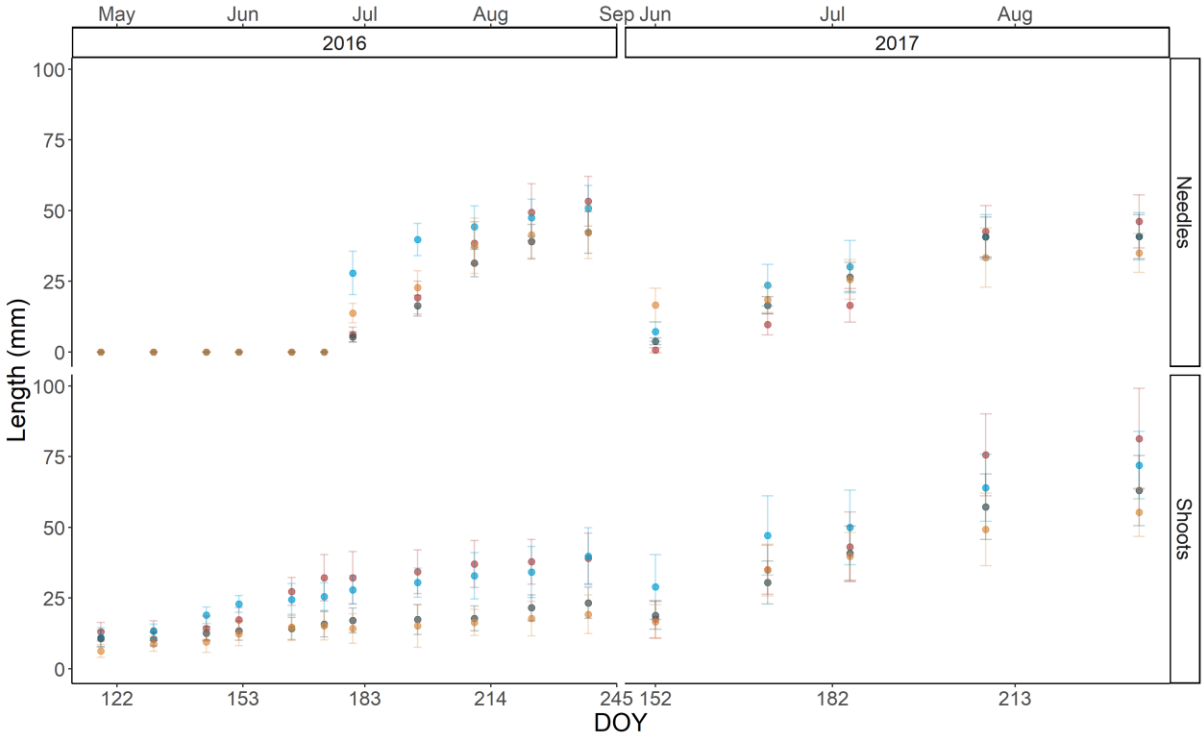

Figure A.6. Boxplots of related soil temperature and xylogenesis variables: (a) soil warming onset, (b) tracheid maturation onset, (c) tracheid maturation duration and (d) rate of production of mature tracheids. In grey, plot 4 was highlighted since it presented "outlier" microclimate conditions and growth characteristics.

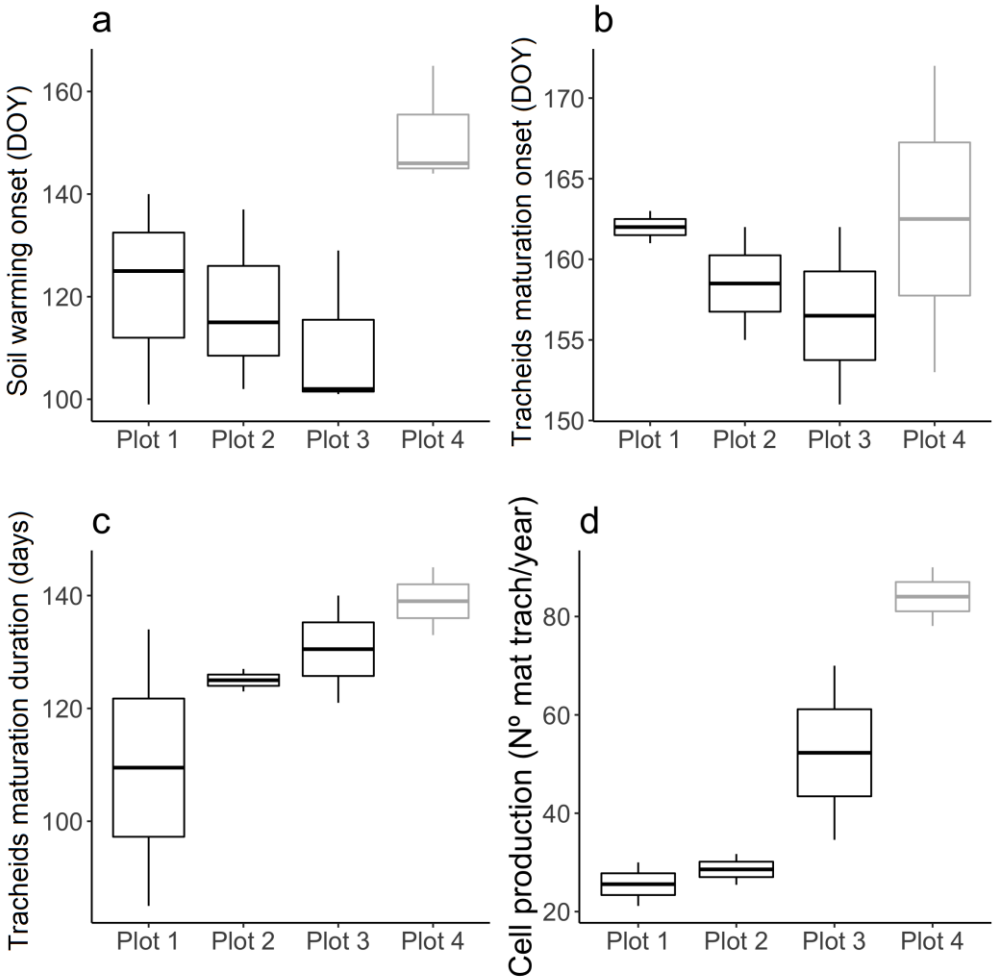

986 **Table A.1.** Descriptive indices calculated from tree growth data.
987

	Index	Description
Stem radial increment	Total stem radial increment	Parameter *A* of Gompertz function adjusted to daily maximum radius series (upper asymptote).
	Stem radial increment onset	Date when daily rates of radial increment exceeded 3 μm·day^{-1}.
	Stem radial increment cessation	Date when daily rates of radial increment fell below 3 μm·day^{-1}.
	Stem radial increment duration	Time between the onset and cessation dates of stem radial increment.
	Maximum rate of radial increment	Maximum value obtained from estimated daily rates of radial increment series.
	Timing of maximum rate of radial increment	Date when maximum rate of radial increment was reached.
Mature tracheids	Production of mature tracheids	Parameter *A* of Gompertz function adjusted to mature cell number increase series (upper asymptote); i.e. number of mature tracheids developed per year.
	Maturation onset	Date when first mature tracheid was completely developed, obtained from Gompertz function adjusted to mature cell number increase series.
	Maturation cessation	Date when last mature tracheid was completely developed, obtained from Gompertz function adjusted to mature cell number increase series.
	Maturation duration	Time between the onset and cessation dates of tracheid maturation.
	Maximum rate of mature tracheid development	Maximum value obtained from estimated daily rates of mature tracheid development series.
	Timing of maximum rate of mature tracheid development	Date when maximum rate of mature tracheid development was reached.
Shoot and needle phenology	Onset of shoot elongation	First day when an increment in shoot length was recorded after dormancy.
	Shoots final lenght	Maximum shoot length recorded.
	Onset of needle elongation	First day when an increment in needle length was recorded after dormancy.
	Needle final length	Maximum needle length value recorded.

988

Table A.2. Average microclimate conditions during each year at each plot.

		Snowpack ‡					Soil								Air					
Year	Plot	Accum. Onset (DOY)	Melt out date (DOY)	Duration (days)	SWE peak (mm)	Day of SWE peak (DOY)	Infilt. onset (DOY)	VWC peak ($m^3 \cdot m^{-3}$) †	Day of VWC peak †	VWC during TGS ($m^3 \cdot m^{-3}$)	Min VWC ($m^3 \cdot m^{-3}$)	Day of min VWC (DOY)	Warming (DOY)	T during TGS (ºC)	Cooling (DOY)	Warming (DOY)	Duration of TGS (days)	T during TGS (ºC)	Cooling (DOY)	H during TGS (%)
2016	1	2	115	114	309	47	7	0.24	130	0.10	0.01	252	125	11.7	311	125	184	11.6	309	63.6
	2	347	117	137	301	80	350	0.29	130	0.14	0.04	252	115	12.2	311	108	201	11.5	309	62.7
	3	2	111	110	144	75	3	0.58	91	0.24	0.06	252	107	10.9	326	107	202	12.5	309	62.4
	4	347	151	171	637	104	350	0.41	130	0.15	0.03	252	144	11.2	286	138	147	11.7	285	60.3
2017	1	2	88	86	350	45	11	0.21	132	0.12	0.05	235	98	9.3	312	68	240	10.4	308	62.4
	2	328	99	137	306	37	339	0.27	132	0.15	0.08	235	101	9.6	310	68	240	11.0	308	61.6
	3	11	101	90	234	38	14	0.50	133	0.29	0.08	291	101	9.5	330	67	241	11.7	308	61.2
	4	319	146	193	721	85	322	0.28	132	0.15	0.05	235	145	7.7	293	70	238	9.2	308	60.8
2018	1	336	128	158	526	101	348	0.28	99	0.14	0.05	248	139	9.9	308	109	191	11.1	300	72.1
	2	336	126	156	575	80	342	0.37	98	0.18	0.08	218	136	10.9	308	107	193	11.8	300	71.2
	3	336	126	156	331	91	342	0.56	99	0.34	0.11	248	128	10.6	324	107	193	12.4	300	71.4
	4	310	154	210	933	102	329	0.34	129	0.17	0.06	219	164	9.0	300	110	189	10.0	299	70.6

(‡) To calculate snow indices, snow seasons temporality was taken into account, not natural years (see Figure A.1.).

(†) The first peaks of soil moisture at plot 1, plot 2 and plot 3 during 2017 snow season were not considered because they preceded snow accumulation (explained by an extraordinary precipitation event in November 2017, see Figure A.3.), thus the second peak was shown here and used in analysis.

Abbreviations: Accum. : Accumulation; SWE: Snow Water Equivalent, Infilt.: Infiltration, VWC: Volumetric water content, Min: minimum, T: temperature; TGS: Thermal growing season; H: humidity

Table A.3. Variance accounted for (%) the two first principal components (PC1 and PC2) and correlations between them and original variables (weekly average microclimate conditions and weekly maximum growth rates). Values in bold indicate the two variables which contributed the most to each PC.

Variable	PCA 1: mature tracheid production		PCA 2: stem radial increment	
	PC1 (55.3%)	PC2 (18.6%)	PC1 (49.9%)	PC2 (22.1%)
Soil T	0.54	-0.18	0.57	-0.14
Soil VWC	-0.38	0.23	-0.42	-0.29
Air T	**0.55**	0.11	**0.58**	-0.18
Air H	-0.27	**-0.90**	-0.39	-0.27
Daily growth rate	0.43	-0.29	0.06	**-0.89**